Available online at www.sciencedirect.com
ScienceDirect
Journal of Solid State Chemistry 180 (2007) 3408–3424
JOURNAL OF SOLID STATE CHEMISTRY
www.elsevier.com/locate/jssc

High-pressure structural evolution of a perovskite solid solution $(La_{1-x},Nd_x)GaO_3$

R.J. Angel[a,*], J. Zhao[a], N.L. Ross[a], C.V. Jakeways[b], S.A.T. Redfern[b], M. Berkowski[c]

[a]*Crystallography Laboratory, Department of Geosciences, Virginia Polytechnic Institute and State University, Blacksburg, VA 24061, USA*
[b]*Department of the Earth Sciences, Cambridge University, UK*
[c]*Institute of Physics, Polish Academy of Sciences, Al. Lotnikow 32/46, 02-668 Warszawa, Poland*

Received 22 November 2006; received in revised form 18 September 2007; accepted 18 September 2007
Available online 25 September 2007

Abstract

The structural evolution with pressure of six perovskites in the system $La_{1-x}Nd_xGaO_3$ with $x = 0.00$, 0.06, 0.12, 0.20, 0.62 and 1.00 have been determined by single-crystal diffraction. At room pressure, all six samples have *Pbnm* symmetry. The room-pressure bulk moduli vary only slightly with composition, between $K_{0T} = 169(4)$ and 177(2) GPa, with $K'_0 = (dK/dP)_{P=0} \sim 6.5$. As pressure is increased there is significant compression of the octahedral Ga–O bonds, the tilts of the GaO_6 octahedra decrease and the structures evolve towards higher symmetry. At room conditions the average Ga–O bond length increases with increasing compositional parameter x. However, the GaO_6 become stiffer with increasing x; the Ga–O bonds thus become *stiffer* as they become *longer*. Bond strengths in the octahedra in perovskites are therefore not a simple function of bond lengths but depend also upon the extra-framework cation.

Phase transitions to *R-3c* symmetry occur at 2.2 GPa in end-member $LaGaO_3$, at ~5.5 GPa in the $x = 0.06$ sample, at ~7.8 GPa for $x = 0.12$, and at ~12 GPa for $x = 0.20$. No evidence of the transition in the $x = 0.62$ or 1.00 samples was found by X-ray diffraction to 9.4 or 8.0 GPa, respectively, or by Raman measurements of $NdGaO_3$ up to 16 GPa. The transition pressure therefore increases with increasing Nd content (increasing x) at approximately 0.45 GPa per 0.01 increment in x, at least up to $x = 0.20$. Compression of the *R-3c* phase of $LaGaO_3$ above the transition results in no significant changes in the tilt angle of the octahedra. The structural behavior of all six samples at high pressures is the result of the GaO_6 octahedra being softer than the extra-framework $(La,Nd)O_{12}$ site. The results therefore demonstrate that the evolution of solid-solution perovskites at high pressures follow the same general principles recently elucidated for end-member compositions.

Keywords: Perovskites; Phase transitions; High pressure; Solid solutions

1. Introduction

The relationship between crystal chemistry, structure and properties of perovskites is becoming ever more important as the range of uses for these ceramics becomes even broader, especially if one wants to pre-design perovskites with specific properties for a practical application. For example, the $(La,Nd)GaO_3$ perovskites with *Pbnm* symmetry that were used in this study have become widely used substrate materials in the last decade because of their low lattice mismatch with high temperature superconductor (HTSC) films which is maintained even at high temperatures [1–5]. Tailoring elasticity and thermal expansion of such perovskites by adjusting the composition requires a detailed and systematic link to be developed between the crystal chemistry and their physical and thermodynamic properties.

Such a link has begun to be established between the crystal chemistry of end-member stoichiometric ABO_3 perovskites and both their elastic properties and structural evolution with pressure. Recent single-crystal X-ray diffraction studies, along with previous research work, clearly indicate that the relative compressibilities of the A and B sites play an important role in determining the pressure-induced structural changes of perovskites [6–17].

*Corresponding author. Fax: +1 540 231 3386.
E-mail address: rangel@vt.edu (R.J. Angel).

0022-4596/$ - see front matter © 2007 Elsevier Inc. All rights reserved.
doi:10.1016/j.jssc.2007.09.019

When the BO_6 octahedra are less compressible than the extra-framework AO_{12} sites the application of pressure leads to increased tilts of the octahedra within a single phase, or to phase transitions to perovskites with lower symmetries and larger tilts. Such behavior is generally observed in perovskites with a cation of +4 formal charge in the octahedral site, and hence a +2 cation in the A site (e.g. $MgSiO_3$ [9], $CaSnO_3$ [14], etc.). This is also the behavior expected from the traditional model of perovskites that considers them comprised of rigid octahedra free only to undergo relative rotations and tilts. By contrast, in perovskites with both cations with +3 formal charges, exactly the opposite high-pressure behavior is observed. The BO_6 octahedra are found to be more compressible than the extra-framework AO_{12} sites. As a consequence, the tilts of the octahedra decrease with increasing pressure [11,12] and can lead to phase transitions to perovskites of higher symmetry. $LaAlO_3$ with *R-3c* symmetry thus exhibits decreasing octahedral tilts with increasing pressure [15] prior to a phase transition to a structure with *Pm3m* symmetry with no tilts at pressures in excess of 14 GPa [18]. Orthorhombic $LaGaO_3$ also exhibits decreased tilts at elevated pressures prior to a phase transition to *R-3c* symmetry at ~2.2 GPa [19].

These observations can be put on a quantitative basis through application of the concept of bond-valence to the calculation of relative polyhedral compressibilities [16,17]. As a perovskite structure is compressed, the bond lengths to both the A and B cations become shorter. As a consequence the formal bond valences of the individual bonds, calculated using the normal bond-valence parameters derived from room-pressure structures (e.g. [20–22]), increase. If the formal bond-valence sums at the cation sites are calculated for a perovskite structure determined at high pressures it is an experimental observation that the increase over the sums at room pressure is the same in a given structure for both the A and B cation sites. This equipartition of "bond-valence strain" has been called the "bond-valence matching principle" [16]. It follows that the relative compressibilities of the AO_{12} and BO_6 sites in any given perovskite are given by $\beta_B/\beta_A = M_A/M_B$, in which the M_A and M_B are site parameters of the room-pressure structure defined as $M_i = (R_iN/B)\ \exp[(R_0-R_i)/B]$. The implication of this analysis is that the compressibility of the polyhedra is not only dependent upon the bond lengths within the polyhedra, but also upon the other cation polyhedra within the structure.

Although the bond-valence matching principle successfully explains the high-pressure compressional behavior and phase transitions of stoichiometric end-member perovskites, its extension to solid solutions is not straight-forward. First, there is very little available data on the structural response of perovskite solid solutions to high pressure. Second, the bond-valence approach is specifically restricted to structures in which each crystallographic distinct site is only occupied by a single atom type. Thus, it is not clear how the bond-valence approach should be modified for solid solutions. Neither is it clear exactly how the apparent A–O and B–O bond lengths obtained from a solid-solution perovskite by a diffraction experiment actually relate to the true local bond lengths within the structure. Therefore as a first step towards exploring the high-pressure behavior of perovskite solid solutions, we have undertaken a single-crystal X-ray diffraction study of pressure-induced structure changes of six members of the $La_{1-x}Nd_xGaO_3$ perovskite solid solution. This solid solution was chosen because of the availability of high-quality single crystals of homogeneous intermediate compositions, all of which exhibit the same *Pbnm* space group symmetry at room pressure. In addition, the *Pbnm* to *R-3c* phase transition reported in the $LaGaO_3$ end-member [19,23], provides us with the opportunity to also determine the interplay between polyhedral properties and phase transitions in perovskite solid solutions.

2. Experimental

$La_{1-x}Nd_xGaO_3$ single crystals ($x = 0.00$; 0.06; 0.12; 0.20; 0.62; 1.00) were prepared by the Czochralski growth technique [24]. Compositions were determined by electron microprobe analysis and reported in [24]. The relatively large pieces of crystals were cut and polished to plates about 30 μm thick. After careful examination by polarized light microscopy and verification of the absence of twin domains on an optical scale, a selected plate was then cut into smaller pieces about 150 μm × 150 μm in size. X-ray diffraction measurements with both a point detector and a CCD area detector on an Xcalibur-1 diffractometer (Oxford Diffraction) were employed in an attempt to detect finer-scale twinning which was found to be absent from most samples. The improvement in the refinement of the structure of $La_{0.94}Nd_{0.06}GaO_3$ obtained when a small twin fraction was refined indicated that this sample included a small amount of sub-optical scale twin domains. This twinning may account for the slightly anomalous data from this sample. Refinements of structures at ambient pressure are consistent with those previously reported for the $La_{1-x}Nd_xGaO_3$ join [24–27].

These smaller pieces of samples were used in high-pressure studies. The selected crystals were loaded separately on to a 600 μm diameter culet of one anvil of an ETH diamond anvil cell [28]. A 4:1 methanol:ethanol mixture served as the pressure-transmitting medium. A 200 μm thick T301 steel gasket was pre-indented to a thickness of ~90 μm and a hole of 300 μm diameter was drilled in the center of the indented region. A ruby sphere (~20 μm) and quartz were loaded together with crystal as the internal pressure calibrants [29,30]. All unit cell parameters were determined by a least-squares fit to the corrected setting angles of 18–20 reflections measured by the eight-position centering technique on a Huber four-circle diffractometer [30].

Intensity data for all accessible reflections were collected at room pressure and at different pressures for all samples

Table 1a
Refinement information, unit cell parameters and refined positional parameters and anisotropic displacement parameters (βij) of *Pbnm* $LaGaO_3$ perovskite at high pressure

P (GPa)	0.0001	1.283(11)	2.038(10)
N_{obs} ($I>2I_0/\sigma(I_0)$)[a]	751	811	737
N_{ind} ($F^2>2\sigma(F^2)$[b]	300	294	292
R_{int}[c]	0.063	0.059	0.054
G_{fit}[d]	1.03	1.17	1.00
N_{int}[e]	299	294	292
Weight, p[f]	0.00	0.00	0.00
Extinction $\times 10^{-4}$[g]	0.098(10)	0.075(7)	0.065(5)
R_w[h]	0.039	0.043	0.035
R_{uw}[i]	0.032	0.033	0.024
a (Å)	5.52288(19)	5.51402(21)	5.50819(20)
b (Å)	5.49293(28)	5.47813(18)	5.46937(17)
c (Å)	7.77302(29)	7.75004(35)	7.73832(29)
V (Å^3)	235.808(15)	234.102(15)	233.127(13)
La(Nd): B_{eq}	0.630(17)	0.59(2)	0.503(16)
x	0.00447(5)	0.00436(6)	0.00417(5)
y	0.51682(10)	0.51560(10)	0.51455(8)
β_{11}	0.0054(3)	0.0050(2)	0.0053(11)
β_{22}	0.0033(3)	0.0033(3)	0.0061(14)
β_{33}	0.00346(15)	0.0032(2)	0.0026(10)
β_{12}	0.00031(7)	0.00016(7)	−0.0010(9)
Ga:B_{eq}	0.52(3)	0.51(3)	0.39(2)
β_{11}	0.0053(5)	0.0040(4)	0.0030(3)
β_{22}	0.0019(4)	0.0024(5)	0.0020(4)
β_{33}	0.0028(3)	0.0031(4)	0.0023(4)
β_{12}	0.00003(10)	−0.00007(12)	−0.00004(11)
β_{13}	0.00001(7)	0.00004(8)	-0.00001(7)
β_{23}	−0.00001(9)	0.00016(12)	−0.00007(9)
O1: B_{eq}	0.71(6)	0.70(7)	0.66(6)
x	−0.0679(8)	−0.0662(10)	−0.0651(7)
y	−0.0066(8)	−0.0044(9)	−0.0051(7)
β_{11}	0.0065(13)	0.0085(16)	0.00396(16)
β_{22}	0.0054(14)	0.0047(16)	0.0032(3)
β_{33}	0.0027(9)	0.0021(12)	0.00272(15)
β_{12}	0.0000(9)	−0.0009(10)	0.00011(6)
O2: B_{eq}	0.74(5)	0.65(6)	0.62(5)
x	0.2290(5)	0.2302(5)	0.2310(4)
y	0.2719(5)	0.2704(6)	0.2700(5)
z	0.0373(5)	0.0367(6)	0.0367(5)
β_{11}	0.0072(8)	0.0062(8)	0.0052(8)
β_{22}	0.0038(10)	0.0028(11)	0.0032(10)
β_{33}	0.0036(6)	0.0036(8)	0.0035(7)
β_{12}	−0.0021(7)	−0.0016(7)	−0.0010(6)
β_{13}	0.0011(6)	0.0007(6)	0.0010(5)
β_{23}	0.0000(6)	−0.0006(6)	−0.0018(5)

La(Nd): $z=0.25$; $\beta_{13}=\beta_{23}=0$. Ga: $x=0.0$, $y=0.0$, $z=0.0$. O1: $z=0.25$; $\beta_{13}=\beta_{23}=0$.

[a]Number of reflections with $I>2I_0/\sigma(I_0)$.
[b]Number of independent reflections with $F^2>2\sigma(F^2)$.
[c]Internal residual for symmetry-equivalent inflections.
[d]Estimated standard deviation of unit weight observation.
[e]Number of independent reflections used in refinement.
[f]Weight $=(\sigma^2(F_i)+p^2F_i^2)^{-2}$.
[g]Extinction factor.
[h]Weighted $R_w=\left[\sum w(|F_0|-|F_c|)^2/\sum|F_0|^2\right]^{1/2}$.
[i]Unweighted $R_{uw}=\sum||F_0|-|F_c||/\sum|F_0|$.

Table 1b
Interatomic distances (Å), angles (deg), and polyhedral volumes of GaO_6, V_{oct} (Å^3), and LaO_{12}, V_{dod} (Å^3), of Pbnm $LaGaO_3$ perovskite at high pressure

		$LaGaO_3$ (*Pbnm*)		
P (GPa)		0.0001	1.283(11)	2.038(10)
Ga–O1	×2	1.9794(8)	1.9717(10)	1.9677(7)
Ga–O21	×2	1.9786(23)	1.9713(26)	1.9699(20)
Ga–O22	×2	1.9731(22)	1.9688(26)	1.9643(20)
⟨GaO_6⟩		1.9770(9)	1.9706(10)	1.9673(8)
V_{oct}		10.298	10.198	10.146
$V_{oct.reg}$*		10.303(14)	10.203(16)	10.152(12)
O1–Ga–O2	×2	89.49(14)	89.23(17)	89.24(13)
O1–Ga–O2	×2	90.69(14)	90.56(17)	90.79(13)
O1–Ga–O1	×2	180.00	180.00	180.00
O1–Ga–O2	×2	89.31(14)	89.44(17)	89.21(13)
O1–Ga–O2	×2	90.51(14)	90.77(17)	90.76(13)
O2–Ga–O2	×2	91.55(3)	91.57(3)	91.60(3)
O2–Ga–O2	×2	90.51(15)	90.77(18)	90.76(15)
O2–Ga–O2	×2	88.45(3)	88.43(3)	88.40(3)
O2–Ga–O2	×2	180.00	180.00	180.00
La(Nd)–O1 i		2.415(4)	2.418(5)	2.421(4)
La(Nd)–O1 ii		2.648(4)	2.658(4)	2.655(4)
La(Nd)–O1 iii		2.903(4)	2.875(5)	2.868(4)
La(Nd)–O1 iv		3.114(4)	3.100(5)	3.091(4)
La(Nd)–O2 v	×2	2.466(3)	2.467(4)	2.465(3)
La(Nd)–O2 vi	×2	2.6202(26)	2.6123(29)	2.6086(25)
La(Nd)–O2 vii	×2	2.8274(27)	2.825(3)	2.8262(28)
La(Nd)–O2 viii	×2	3.133(3)	3.111(4)	3.100(3)
⟨LaO_{12}⟩		2.764(4)	2.757(5)	2.753(4)
⟨LaO_8⟩		2.611(4)	2.611(5)	2.609(4)
⟨LaO_4⟩		3.071(4)	3.049(5)	3.040(4)
V_{dod}		48.649(28)	48.322(32)	48.130(24)
Ga–O1–Ga		158.07(22)	158.62(31)	158.95(21)
Ga–O2–Ga		160.51(20)	161.04(24)	161.18(20)

*The regular octahedral volume $V_{oct,reg}$ is calculated as $V_{oct,reg}=\frac{4}{3}GaO_1\times GaO_{21}\times GaO_{22}$ and corresponds to an octahedron with all O–Ga–O bond angles 90° or 180°. Uncertainty of V_{oct} is probably overestimated by that of $V_{oct,reg}$.

using an Xcalibur-1 diffractometer equipped with a point detector and a Mo $K\alpha$ radiation source run at 50 kV and 40 mA. Prior to each intensity data collection, the offsets of the crystal from the center of the goniometer were determined by measuring 20–40 strong low-angle reflections and calculating the crystal offsets from the reflection positions with the WinIntegrStp program [31]. These offsets were then minimized by adjusting DAC on the goniometer before data collection. The intensities of all accessible reflections from 2° to 40° in θ were measured with constant-precision step-scans in ω with the diamond-anvil cell set in fixed-ϕ mode [32]. Peak fitting and integration of data collection scans were carried out by using the WinIntegrStp software. Other data corrections including absorption by the sample itself, the beryllium plates and diamond anvils of the DAC as well as shadowing by the gasket were made by ABSORB 6.0 [33]. After the crystallographically equivalent reflections were averaged and outliers excluded, the remaining independent reflections with $F^2>2\sigma(F^2)$ were used to refine structures with RFINE99, a development version of RFINE4 [34]. Unit cell parameters measured on Huber

Table 2a
Refinement information, unit cell parameters and refined positional parameters of *Pbnm* $La_{0.94}Ga_{0.06}O_3$ perovskite at high pressure

P (GPa)	0.0001	0.967(2)	2.56(5)	3.98(5)	5.30(5)
N_{obs} ($I>2I_0/\sigma(I_0)$)	677	669	652	658	583
N_{ind} ($F^2>2\sigma(F^2)$)	152	153	175	186	175
R_{int}	0.061	0.062	0.055	0.066	0.065
G_{fit}	1.13	1.16	1.00	1.08	1.14
N_{int}	153	151	170	182	172
Weight, p	0.03	0.03	0.00	0.03	0.03
Extinction $\times 10^{-4}$	0.18(2)	0.19(2)	0.16(10)	0.18(2)	0.20(2)
R_w	0.056	0.062	0.037	0.060	0.062
R_{uw}	0.033	0.036	0.033	0.042	0.045
a (Å)	5.5124(5)	5.5054(4)	5.4980(5)	5.4870(4)	5.4789(3)
b (Å)	5.4936(2)	5.4819(2)	5.4625(9)	5.4445(6)	5.4311(2)
c (Å)	7.7706(8)	7.7547(9)	7.7327(17)	7.7067(15)	7.6837(8)
V (Å^3)	235.32(4)	234.04(3)	232.23(6)	230.23(5)	228.64(3)
La(Nd): B_{eq}	0.53(3)	0.53(4)	0.49(3)	0.45(3)	0.52(4)
x	0.00491(10)	0.00490(11)	0.00453(8)	0.00420(10)	0.00406(11)
y	0.5200(3)	0.5190(3)	0.51677(13)	0.51523(18)	0.51320(17)
Ga: B_{eq}	0.50(4)	0.53(5)	0.38(3)	0.33(4)	0.43(5)
O1: B_{eq}	0.60(13)	0.87(17)	0.67(12)	0.45(13)	0.60(16)
x	−0.0682(14)	−0.0669(17)	−0.0667(12)	−0.0647(14)	−0.0660(17)
y	−0.0072(14)	−0.0081(16)	−0.0102(12)	−0.0064(14)	−0.0055(15)
O2: B_{eq}	0.39(9)	0.58(11)	0.53(9)	0.57(11)	0.57(14)
x	0.2253(8)	0.2258(9)	0.2284(7)	0.2302(8)	0.2311(9)
y	0.2749(8)	0.2728(9)	0.2724(7)	0.2709(9)	0.2674(10)
z	0.0400(12)	0.0393(16)	0.0382(11)	0.0377(14)	0.0400(15)

Isotropic temperature factor (B_{eq}) were used in the refinements.

Table 2b
Interatomic distances, angles, and polyhedral volumes of *Pbnm* $La_{0.94}Nd_{0.06}GaO_3$ perovskite at high pressure

P (GPa)		0.0001	0.967(2)	2.56(5)	3.98(5)	5.30(5)
Ga–O1	×2	1.9791(14)	1.9739(16)	1.9684(11)	1.9594(13)	1.9549(17)
Ga–O21	×2	1.980(4)	1.968(5)	1.969(4)	1.963(4)	1.951(5)
Ga–O22	×2	1.979(4)	1.981(5)	1.967(4)	1.958(4)	1.965(5)
$\langle GaO_6\rangle$		1.9794(15)	1.9743(20)	1.9681(15)	1.9601(15)	1.9570(20)
V_{oct}		10.333	10.253	10.152	10.034	9.982
$V_{oct,\ reg}$		10.340(24)	10.26(3)	10.164(23)	10.041(23)	9.99(3)
O1–Ga–O2	×2	88.88(26)	89.03(36)	89.58(26)	89.10(34)	88.66(38)
O1–Ga–O2	×2	91.22(24)	91.30(33)	91.37(26)	91.16(33)	91.43(37)
O1–Ga–O1	×2	180.00	180.00	180.00	180.00	180.00
O1–Ga–O2	×2	88.78(24)	88.70(33)	88.63(26)	88.84(33)	88.57(37)
O1–Ga–O2	×2	91.12(26)	90.97(36)	90.42(26)	90.90(34)	91.34(38)
O2–Ga–O2	×2	91.60(08)	91.57(10)	91.67(07)	91.71(09)	91.87(10)
O2–Ga–O2	×2	91.12(33)	90.97(41)	90.42(29)	90.90(37)	91.34(41)
O2–Ga–O2	×2	88.40(08)	88.43(10)	88.33(07)	88.29(09)	88.13(10)
O2–Ga–O2	×2	180.00	180.00	180.00	180.00	180.00
La(Nd)–O1 i		2.412(8)	2.416(9)	2.412(6)	2.415(7)	2.402(9)
La(Nd)–O1 ii		2.629(8)	2.623(8)	2.614(6)	2.632(8)	2.642(8)
La(Nd)–O1 iii		3.109(8)	3.098(9)	3.094(6)	3.077(7)	3.081(9)
La(Nd)–O1 iv		2.924(8)	2.916(8)	2.905(6)	2.865(8)	2.843(8)
La(Nd)–O2 v	×2	2.440(7)	2.443(9)	2.445(6)	2.446(8)	2.436(9)
La(Nd)–O2 vi	×2	2.615(6)	2.609(8)	2.605(5)	2.596(7)	2.572(8)
La(Nd)–O2 vii	×2	2.821(7)	2.819(9)	2.817(6)	2.815(8)	2.837(9)
La(Nd)–O2 viii	×2	3.174(8)	3.155(10)	3.125(7)	3.099(9)	3.086(9)
$\langle La(Nd)O_{12}\rangle$		2.765(9)	2.759(9)	2.751(7	2.742(9)	2.735(9)
$\langle La(Nd)O_8\rangle$		2.599(9)	2.598(9)	2.595(7	2.595(9)	2.592(9)
$\langle La(Nd)O_4\rangle$		3.095(8)	3.081(10)	3.062(7)	3.035(9)	3.024(9)
V_{dod}		48.50(5)	48.26(6)	47.91(5)	47.53(5)	47.18(6)
Ga–O1–Ga		158.0(4)	158.3(5)	158.2(4)	159.0(4)	158.6(5)
Ga–O2–Ga		158.7(5)	159.2(6)	160.0(4)	160.5(6)	160.1(6)

diffractometer were used in the structure refinements. Refinement information, bond distances, angles and unit cell parameters for the $La_{1-x}Nd_xGaO_3$ samples at high pressure are listed in Tables 1–9.

The phase transition from *Pbnm* symmetry to *R-3c* in $LaGaO_3$ and La-rich members of the (La, Nd)GaO_3 solid solution is marked at high temperature by a decrease in the number of bands from ~18 to 4 [26,35]. We found that non-polarized Raman measurements from un-oriented single-crystal chips of samples with $x=0.00$, 0.06, 0.12 revealed similar distinct changes at the pressures corresponding to the high-pressure transitions detected by single-crystal diffraction, although details of the spectra depend on, of course, sample orientation.

Table 3a
Refinement information, unit cell parameters and refined positional parameters and anisotropic displacement parameters (β_{ij}) of *Pbnm* $La_{0.88}Nd_{0.12}GaO_3$ perovskite at high pressure

P (GPa)	0.0001	4.497(6)	6.437(7)
N_{obs} ($I>2I_0/\sigma(I_0)$)	601	593	553
N_{ind} ($F^2>2\sigma(F^2)$)	264	262	249
R_{int}	0.052	0.036	0.052
G_{fit}	1.08	1.20	1.05
N_{int}	262	260	246
Weight, p	0.03	0.01	0.01
Extinction $\times 10^{-4}$	0.091(13)	0.060(8)	0.078(9)
R_w	0.056	0.042	0.042
R_{uw}	0.034	0.031	0.031
a (Å)	5.5128(4)	5.48116(29)	5.46878(23)
b (Å)	5.4928(4)	5.4425(4)	5.4235(3)
c (Å)	7.7732(7)	7.6997(5)	7.6695(4)
V (Å^3)	235.38(3)	229.691(23)	227.477(18)
La(Nd): B_{eq}	0.71(3)	0.53(3)	0.62(3)
x	0.00490(9)	0.00428(8)	0.00401(8)
y	0.51908(16)	0.51564(10)	0.51357(10)
β_{11}	0.0058(4)	0.0047(3)	0.0059(3)
β_{22}	0.0059(4)	0.0044(3)	0.0053(3)
β_{33}	0.0029(2)	0.00211(16)	0.00223(17)
β_{12}	0.00019(13)	0.00018(15)	0.00002(16)
Ga: B_{eq}	0.56(4)	0.42(3)	0.48(3)
β_{11}	0.0040(6)	0.0039(4)	0.0055(5)
β_{22}	0.0057(6)	0.0037(4)	0.0044(4)
β_{33}	0.0022(4)	0.0015(3)	0.0010(3)
β_{12}	0.0002(3)	−0.0002(3)	−0.0010(4)
β_{13}	−0.00006(11)	−0.00001(10)	−0.00009(11)
β_{23}	−0.00009(16)	0.00008(12)	0.00009(10)
O1: B_{eq}	1.25(13)	0.69(10)	0.87(10)
x	−0.0663(14)	−0.0678(13)	−0.0649(13)
y	−0.0087(17)	−0.0059(11)	−0.0066(11)
β_{11}	0.008(3)	0.0079(19)	0.008(2)
β_{22}	0.018(4)	0.007(3)	0.011(3)
β_{33}	0.0023(14)	0.0014(14)	0.0014(13)
β_{12}	−0.0027(19)	−0.0017(14)	−0.0003(14)
O2: B_{eq}	0.83(9)	0.73(9)	0.73(7)
x	0.2268(8)	0.2283(7)	0.2304(8)
y	0.2751(8)	0.2718(6)	0.2693(7)
z	0.0376(8)	0.0369(8)	0.0373(7)
β_{11}	0.0075(16)	0.0064(15)	0.0043(17)
β_{22}	0.0022(18)	0.0044(15)	0.0044
β_{33}	0.0054(9)	0.0037(11)	0.0049(9)
β_{12}	−0.0006(11)	−0.0027(10)	−0.0027
β_{13}	0.0031(9)	0.0010(9)	0.0002(10)
β_{23}	−0.0003(9)	−0.0038(10)	−0.0033(9)

Table 3b
Interatomic distances, angles, and polyhedral volumes of *Pbnm* $La_{0.88}Nd_{0.12}GaO_3$ perovskite at high pressure

P (GPa):		0.0001	4.497(6)	6.437(7)
Ga–O1	×2	1.9779(13)	1.9607(13)	1.9502(12)
Ga–O21	×2	1.983(4)	1.958(3)	1.950(4)
Ga–O22	×2	1.970(4)	1.960(3)	1.955(4)
⟨GaO_6⟩		1.9768(16)	1.9596(12)	1.9517(15)
V_{oct}		10.296	10.015	9.904
$V_{oct,reg}$		10.300(25)	10.033(18)	9.912(23)
O1–Ga–O2	×2	89.44(26)	89.48(22)	89.25(18)
O1–Ga–O2	×2	91.12(26)	90.49(22)	91.06(18)
O1–Ga–O1	×2	180.00	180.00	180.00
O1–Ga–O2	×2	88.88(26)	89.51(22)	88.94(18)
O1–Ga–O2	×2	90.56(26)	90.52(22)	90.75(18)
O2–Ga–O2	×2	91.49(5)	91.60(5)	91.69(4)
O2–Ga–O2	×2	90.56(29)	90.52(24)	90.75(23)
O2–Ga–O2	×2	88.51(5)	88.40(5)	88.31(4)
O2–Ga–O2	×2	180.00	180.00	180.00
La(Nd)–O1 i		2.423(7)	2.395(7)	2.404(7)
La(Nd)–O1 ii		2.624(9)	2.634(6)	2.629(6)
La(Nd)–O1 iii		2.925(9)	2.866(6)	2.846(6)
La(Nd)–O1 iv		3.099(7)	3.091(7)	3.069(7)
La(Nd)–O2 v	×2	2.453(5)	2.442(4)	2.439(4)
La(Nd)–O2 vi	×2	2.625(4)	2.605(5)	2.587(4)
La(Nd)–O2 vii	×2	2.812(5)	2.800(5)	2.808(4)
La(Nd)–O2 viii	×2	3.156(5)	3.101(5)	3.074(5)
⟨$La(Nd)O_{12}$⟩		2.764(9)	2.740(7)	2.730(7)
⟨$La(Nd)O_8$⟩		2.603(9)	2.590(7)	2.588(7)
⟨$La(Nd)O_4$⟩		3.084(9)	3.040(7)	3.016(7)
V_{dod}		48.55(5)	47.40(4)	46.97(5)
Ga–O1–Ga		158.5(4)	158.1(4)	158.9(4)
Ga–O2–Ga		159.8(3)	160.6(3)	160.9(3)

3. Results

3.1. EoS and unit-cell parameters

The unit-cell parameters and unit-cell volumes of the *Pbnm* phases of all six compositions vary smoothly with pressure (Fig. 1). The first-order phase transitions to the *R-3c* phase in La-rich samples are marked by a significant change in the lattice metric and a first-order step in the unit-cell volume. The transition occurs between 2.15 and 2.36 GPa in $LaGaO_3$ [19,23], and at higher pressures as Nd is substituted for La. The transition pressure as determined by X-ray diffraction for the $x=0.06$ sample is ~5.5 GPa and for $x=0.12$ is ~7.8 GPa. The transition was not observed by X-ray diffraction measurements in the $x=0.20$ and 0.62 samples or pure $NdGaO_3$, so the transition pressures are above ~10 GPa, in agreement with a previous computer simulation [36]. The transitions and the evolution of the *R-3c* phase with pressure are discussed in more detail below.

Table 4a
Refinement information, unit cell parameters and refined positional parameters and anisotropic displacement parameters (β_{ij}) of *Pbnm* $La_{0.80}Nd_{0.20}GaO_3$ perovskite at high pressure

P (GPa)	0.0001	2.619(4)	4.172(3)	8.166(8)	8.671(7)
N_{obs} ($I>2I_0/\sigma(I_0)$)	702	681	653	646	625
N_{ind} ($F^2>2\sigma(F^2)$)	208	205	195	203	189
R_{int}	0.048	0.037	0.039	0.040	0.038
G_{fit}	0.91	1.13	1.11	1.00	1.17
N_{int}	208	205	192	203	189
Weight, p	0.0	0.01	0.015	0.00	0.01
Extinction $\times 10^{-4}$	0.073(8)	0.078(9)	0.069(9)	0.086(7)	0.082(9)
R_w	0.027	0.035	0.038	0.030	0.037
R_{uw}	0.022	0.027	0.026	0.028	0.029
a (Å)	5.50601(20)	5.48675(17)	5.47611(15)	5.45111(27)	5.44834(20)
b (Å)	5.49275(23)	5.46226(20)	5.44520(18)	5.4066(3)	5.40161(25)
c (Å)	7.7673(4)	7.7262(3)	7.70291(29)	7.6463(5)	7.6399(4)
V (Å^3)	234.906(14)	231.556(12)	229.689(10)	225.349(19)	224.841(14)
La(Nd): B_{eq}	0.46(2)	0.41(3)	0.37(3)	0.39(2)	0.34(3)
X	0.00543(6)	0.00507(8)	0.00488(7)	0.00412(6)	0.00407(8)
Y	0.52321(10)	0.52083(12)	0.51959(13)	0.51554(9)	0.51513(12)
β_{11}	0.00385(15)	0.00334(18)	0.00305(19)	0.00346(14)	0.0031(2)
β_{22}	0.0040(3)	0.0041(4)	0.0040(4)	0.0041(3)	0.0040(4)
β_{33}	0.0017(3)	0.0014(4)	0.0011(4)	0.0011(3)	0.0008(5)
β_{12}	0.00049(8)	0.00038(12)	0.00051(14)	0.00036(11)	0.00009(15)
Ga: B_{eq}	0.46(2)	0.32(4)	0.28(5)	0.27(4)	0.29(5)
β_{11}	0.0030(3)	0.0027(3)	0.0024(4)	0.0028(3)	0.0027(4)
β_{22}	0.0026(5)	0.0024(6)	0.0023(8)	0.0025(5)	0.0019(8)
β_{33}	0.0016(6)	0.0014(7)	0.0012(8)	0.0008(7)	0.0015(9)
β_{12}	0.00033(13)	0.0001(3)	−0.0001(3)	−0.0002(2)	0.0006(3)
β_{13}	−0.00002(13)	−0.00021(17)	−0.0001(3)	0.00000(14)	−0.00005(19)
β_{23}	0.00022(14)	0.00009(16)	0.00012(15)	0.00015(13)	0.00021(16)
O1: B_{eq}	0.48(15)	0.44(15)	0.67(9)	0.84(19)	0.66(10)
x	−0.0688(8)	−0.0683(10)	−0.0696(11)	−0.0686(9)	−0.0668(11)
y	−0.0099(9)	−0.0091(11)	−0.0091(13)	−0.0062(9)	−0.0059(11)
β_{11}	0.0054(12)	0.0054(16)	0.0044(14)	0.0049(13)	0.0046(15)
β_{22}	0.005(3)	0.0025(18)	0.002(3)	0.005(3)	0.001(3)
β_{33}	0.001(3)	0.0022(19)	0.0016(18)	0.006(4)	0.002(3)
β_{12}	0.0002(11)	−0.0015(15)	−0.0017(17)	−0.0010(14)	−0.0004(16)
O2: B_{eq}	0.47(11)	0.50(13)	0.61(14)	0.64(13)	0.47(8)
x	0.2238(5)	0.2241(6)	0.2255(6)	0.2294(6)	0.2294(6)
y	0.2777(7)	0.2763(7)	0.2748(9)	0.2715(6)	0.2709(8)
z	0.0385(5)	0.0376(8)	0.0383(8)	0.0380(7)	0.0390(7)
β_{11}	0.0054(8)	0.0055(12)	0.0053(11)	0.0039(9)	0.0058(13)
β_{22}	0.0037(17)	0.002(3)	0.003(3)	0.0027(18)	0.0034(16)
β_{33}	0.0013(18)	0.002(3)	0.003(3)	0.004(3)	0.0033(18)
β_{12}	−0.0013(8)	−0.0021(10)	−0.0028(12)	−0.0026(9)	−0.0023(12)
β_{13}	0.0005(7)	0.0028(10)	0.0028(10)	0.0005(9)	0.0027(11)
β_{23}	−0.0005(5)	−0.0002(8)	−0.0008(9)	−0.0004(7)	−0.0014(10)

Within the stability field of the *Pbnm* phases at high pressure the unit-cell parameters show no evidence of softening as the phase transition pressure is approached, in contrast to softening observed in both continuous and first-order transitions at high pressures in other systems (e.g. [37,38]). The volume variation of the more Nd-rich samples ($x=0.12$, 0.20, 0.62, 1.00) can be adequately fit with a Birch–Murnaghan third-order equation of state [39]. In common with other *Pbnm* perovskites [12,13], the pressure derivative of the bulk modulus, $K'_0=(dK/dP)_{P=0}$, is in the range of 6–7. For the La-rich samples ($x=0.00$, 0.06) the phase transitions limit the pressure range over which the unit-cell data can be collected for the *Pbnm* phase, and the refinement of the third-order equation of state is not stable. We therefore fixed the value of K'_0 in fitting the P–V data for these two samples to the average of that of the Nd-rich samples. The results (Table 10) show that the bulk modulus increases by about 4% across the solid solution from $LaGaO_3$ to $NdGaO_3$ (Fig. 2), which is to be expected for the corresponding ~2% decrease in unit-cell volume (Table 1 in [24]). The bulk modulus that we obtain for $NdGaO_3$ is about 5% lower than that measured experimentally [40 quoted in 27], and that obtained from the elastic constant tensor calculated through MD simulations

Table 4b
Interatomic distances, angles, and polyhedral volumes of *Pbnm* $La_{0.80}Nd_{0.20}GaO_3$ perovskite at high pressure

P (GPa)		0.0001	2.619(4)	4.172(3)	8.166(8)	8.671(7)
Ga–O1	× 2	1.9789(7)	1.9682(10)	1.9637(10)	1.9446(11)	1.9433(11)
Ga–O21	× 2	1.984(3)	1.968(3)	1.962(4)	1.947(3)	1.945(3)
Ga–O22	× 2	1.9729(28)	1.967(3)	1.962(4)	1.948(3)	1.947(3)
$\langle GaO_6 \rangle$		1.9785(11)	1.9678(13)	1.9628(14)	1.9465(12)	1.9451(12)
V_{oct}		10.321	10.156	10.077	9.850	9.826
$V_{oct,reg}$		10.326(17)	10.160(20)	10.082(22)	9.833(18)	9.812(18)
O1-Ga–O2	× 2	89.54(15)	89.61(22)	89.64(22)	88.97(20)	88.96(20)
O1–Ga–O2	× 2	91.04(14)	90.82(24)	90.84(21)	91.10(20)	91.11(20)
O1–Ga–O1	× 2	180.00	180.00	180.00	180.00	180.00
O1–Ga–O2	× 2	88.96(14)	89.18(24)	89.16(21)	88.90(20)	88.89(20)
O1–Ga–O2	× 2	90.46(15)	90.39(22)	90.36(22)	91.03(20)	91.04(20)
O2–Ga–O2	× 2	91.48(04)	91.51(06)	91.61(05)	91.82(05)	91.86(05)
O2–Ga–O2	× 2	90.46(17)	90.39(23)	90.36(24)	91.03(23)	91.04(23)
O2–Ga–O2	× 2	88.52(04)	88.49(06)	88.39(05)	88.18(05)	88.14(05)
O2–Ga–O2	× 2	180.00	180.00	180.00	180.00	180.00
La(Nd)–O1 i		2.411(4)	2.402(5)	2.389(6)	2.385(6)	2.383(6)
La(Nd)–O1 ii		2.597(5)	2.599(6)	2.599(7)	2.616(6)	2.612(6)
La(Nd)–O1 iii		2.956(5)	2.922(6)	2.908(7)	2.841(6)	2.837(6)
La(Nd)–O1 iv		3.107(4)	3.095(5)	3.096(6)	3.068(6)	3.066(6)
La(Nd)–O2 v	× 2	2.442(4)	2.433(5)	2.428(5)	2.418(5)	2.415(5)
La(Nd)–O2 vi	× 2	2.622(3)	2.617(5)	2.602(4)	2.572(4)	2.569(5)
La(Nd)–O2 vii	× 2	2.795(3)	2.784(5)	2.789(5)	2.798(4)	2.797(4)
La(Nd)–O2 viii	× 2	3.187(4)	3.154(5)	3.137(5)	3.083(5)	3.081(4)
$\langle La(Nd)O_{12} \rangle$		2.764 (5)	2.749 (6)	2.742 (7)	2.721(6)	2.719(6)
$\langle La(Nd)O_8 \rangle$		2.591 (5)	2.584 (6)	2.578(7)	2.572 (6)	2.570(6)
$\langle La(Nd)O_4 \rangle$		3.109(5)	3.081(6)	3.070(7)	3.019(6)	3.016(6)
V_{dod}		48.41(3)	47.73(4)	47.35(4)	46.49(4)	46.38(4)
Ga–O1–Ga		157.71(22)	157.85(31)	157.44(32)	158.34(35)	158.31(35)
Ga–O2–Ga		158.72(21)	159.27(31)	159.37(30)	160.00(30)	159.96(30)

[27] of the structure at room conditions. On the other hand, the value of $K_0 = 186.5$ GPa obtained directly from MD simulations of the structure at high pressure [27] is in closer agreement with the current work.

Estimates of the linear moduli of the axes were obtained by fitting the cubes of the unit-cell parameters with the Birch–Murnaghan Eos [41], and full results are provided in Table 10. Again, the limited data range for the La-rich samples precludes a full refinement of all of the EoS parameters so, where necessary, the value of K_0' was constrained to the values determined from the data of more Nd-rich samples. The results of this analysis show that the elasticity of all members of the solid solution is very similar. All six compositions show a similar strong anisotropy of unit-cell compression (Fig. 2), with the [100] direction (the a unit-cell parameter) being approximately 1.6 times stiffer than [010] or [001]. Within the uncertainties the [010] and [001] directions have the same moduli for the La-rich compositions, but the addition of Nd increases the elastic anisotropy in the b–c plane, with the [010] direction being softened and the [001] direction becoming stiffer, so that for $NdGaO_3$ the linear modulus of the [001] direction is some 50 GPa stiffer than that of [010]. The linear compressibilities obtained from the elastic constant tensor calculated from the MD simulations of $NdGaO_3$ [27] reflect the same pattern of anisotropy, but with the one significant difference that their results correspond to a value of $K_{0c} = 250$ GPa compared to the value of 189(2) GPa (Table 10). By contrast, the elastic constant tensor obtained from direct ultrasonic measurements [40] corresponds to the [001] direction being the softest direction with $K_{0c} = 140$ GPa, and with the (001) plane being close to elastically isotropic in compression. Those measurements are therefore not compatible with the data reported here.

3.2. *Pbnm* structure

The structures of all six samples refined to intensity data collected at room pressure inside the diamond-anvil pressure cell are in good agreement with the structures previously determined at room conditions [24–27]. Nonetheless, in order to avoid any systematic errors in the DAC data from affecting the conclusions, the DAC data at room pressure are used as a basis for comparison with the high-pressure data. Both sets of room-pressure data show that there is only small variation in the structure with composition. There is a small but significant increase in

Table 5a
Refinement information, unit cell parameters and refined positional parameters of *Pbnm* $La_{0.38}Nd_{0.62}GaO_3$ perovskite

P (GPa)	In air	0.0001	2.007(5)	4.042(7)	5.188(8)[a]	7.376(11)	8.462(10)	9.432(11)
N_{obs} ($I>2I_0/\sigma(I_0)$)	664	625	567	592	717	664	704	658
N_{ind} ($F^2>2\sigma(F^2)$)	285	252	217	217	269	247	266	230
R_{int}	0.031	0.037	0.034	0.037	0.032	0.036	0.031	0.050
G_{fit}	0.98	1.12	1.20	1.20	1.27	1.09	1.21	1.06
N_{av}	279	249	210	212	267	246	258	226
Weight, p	0.00	0.00	0.05	0.03	0.03	0.03	0.03	0.03
Extinction $\times 10^{-4}$	0.036(5)	0.061(9)	0.084(16)	0.061(12)	0.071(13)	0.077(11)	0.065(11)	0.079(13)
R_w	0.024	0.034	0.055	0.056	0.056	0.052	0.054	0.051
R_{uw}	0.021	0.027	0.031	0.031	0.029	0.031	0.029	0.038
a (Å)	5.4614(6)	5.4614(6)	5.4466(6)	5.4322(5)	5.4238(6)	5.4094(5)	5.4029(5)	5.3968(4)
b (Å)	5.4961(6)	5.4961(6)	5.4697(5)	5.4457(6)	5.4325(6)	5.4092(5)	5.3989(5)	5.3890(5)
c (Å)	7.73893(28)	7.73893(28)	7.71152(25)	7.68457(24)	7.67049(28)	7.64420(28)	7.63119(27)	7.62046(25)
V (Å^3)	232.295(20)	232.295(20)	229.733(19)	227.327(18)	226.008(18)	223.677(19)	222.601(19)	221.630(17)
La(Nd): B_{eq}	0.545(12)	0.65(2)	0.80(4)	0.70(4)	0.61(3)	0.66(3)	0.55(3)	0.63(4)
x	0.00742(4)	0.00757(7)	0.00686(9)	0.00670(9)	0.00647(8)	0.00588(8)	0.00613(8)	0.00585(8)
y	0.53384(12)	0.53346(15)	0.5318(3)	0.5305(3)	0.5294(3)	0.5283(3)	0.5277(3)	0.5274(3)
β_{11}	0.00472(12)	0.0060(3)	0.0065(5)	0.0048(5)	0.0043(3)	0.0041(3)	0.0035(3)	0.0044(4)
β_{22}	0.0047(3)	0.0056(5)	0.0090(10)	0.0083(10)	0.0065(7)	0.0079(8)	0.0062(8)	0.0077(10)
β_{33}	0.00209(6)	0.00231(10)	0.00231(15)	0.00231(16)	0.00238(11)	0.00244(11)	0.00220(12)	0.00215(12)
β_{12}	0.00061(4)	0.00064(8)	0.00076(10)	0.00065(10)	0.00066(9)	0.00048(11)	0.00051(8)	0.00041(10)
Ga: B_{eq}	0.37(3)	0.56(3)	0.65(7)	0.58(7)	0.58(5)	0.60(5)	0.52(5)	0.59(7)
β_{11}	0.0039(3)	0.0053(6)	0.0053(9)	0.0036(8)	0.0037(6)	0.0025(6)	0.0025(6)	0.0041(7)
β_{22}	0.0019(8)	0.0051(8)	0.0073(18)	0.0076(19)	0.0075(14)	0.0094(15)	0.0077(15)	0.008(2)
β_{33}	0.00176(10)	0.00176(16)	0.0018(3)	0.0017(3)	0.0017(2)	0.0018(2)	0.0015(3)	0.0013(3)
β_{12}	0.00002(7)	0.00027(14)	−0.00001(18)	−0.00012(19)	0.00002(17)	0.0005(3)	0.00000(16)	−0.0002(3)
β_{13}	0.00010(5)	−0.00016(9)	−0.00004(13)	−0.00018(10)	−0.00020(10)	−0.00006(10)	−0.00022(9)	0.00012(9)
β_{23}	0.00018(10)	0.00014(16)	0.0002(3)	−0.0001(3)	0.0002(2)	0.0001(3)	−0.0001(2)	0.0006(3)
O1: B_{eq}	0.68(8)	0.84(12)	0.68	0.68	0.68	0.68	0.68	0.68
x	−0.0766(7)	−0.0759(12)	−0.0750(15)	−0.0763	−0.0742(13)	−0.0718(12)	−0.0718(12)	−0.0732(12)
y	−0.0153(6)	−0.0130(12)	−0.0153(15)	−0.0131	−0.0129(18)	−0.011(3)	−0.0114(18)	−0.011(2)
β_{11}	0.0096(13)	0.0096	0.0096	0.0096	0.0096	0.0096	0.0096	0.0096
β_{22}	0.004(3)	0.004	0.004	0.004	0.004	0.004	0.004	0.004
β_{33}	0.0017(4)	0.0017	0.0017	0.0017	0.0017	0.0017	0.0017	0.0017
β_{12}	0.0000(7)	0.0000	0.0000	0.0000	0.0000	0.0000	0.0000	0.0000
O2: B_{eq}	0.85(6)	0.73(8)	0.86(11)	0.85	0.85	0.85	0.85	0.85
x	0.2149(4)	0.2150(6)	0.2181(8)	0.2171(8)	0.2172(7)	0.2186(7)	0.2179(7)	0.2188(7)
y	0.2853(5)	0.2844(8)	0.2825(9)	0.2826(14)	0.2822(15)	0.2803(15)	0.2824(13)	0.2816(13)
z	0.0404(3)	0.0403(5)	0.0392(7)	0.0404(7)	0.0393(7)	0.0394(7)	0.0402(6)	0.0390(7)
β_{11}	0.0085(8)	0.0085	0.0097(18)	0.0085	0.0085	0.0085	0.0085	0.0085
β_{22}	0.0077(16)	0.0077	0.005(3)	0.0077	0.0077	0.0077	0.0077	0.0077
β_{33}	0.0025(3)	0.0025	0.0034(7)	0.0025	0.0025	0.0025	0.0025	0.0025
β_{12}	−0.0018(6)	−0.0018	−0.0010(12)	−0.0018	−0.0018	−0.0018	−0.0018	−0.0018
β_{13}	−0.0002(3)	−0.0002	0.0015(9)	−0.0002	−0.0002	−0.0002	−0.0002	−0.0002
β_{23}	0.0001(4)	0.0001	−0.0005(11)	0.0001	0.0001	0.0001	0.0001	0.0001

High-pressure anisotropic displacement parameters were fixed at the room-pressure values.
[a]The data was measured after decompression from maximum pressure.

octahedral Ga–O bond lengths with increasing Nd content, and the smaller Nd cation is accommodated by greater rotations of the GaO_6 octahedra, represented by larger Ga–O–Ga bond angles ([24–27] and Fig. 3).

The general pattern of structural evolution of all six samples with pressure is similar. Both symmetry-independent Ga–O–Ga angles within each structure increase with pressure, back towards 180°. This corresponds to a decrease in the tilts of the octahedra (Fig. 3). There is significant compression of the Ga–O bonds within the octahedra (Fig. 4), with little significant change in the O–Ga–O angles (Tables 1b–6b), which corresponds to a volume reduction of the GaO_6 octahedra of all six samples as pressure is increased. Similarly, all 12 of the (La, Nd)–O distances to the extra-framework cation site decrease with pressure. When treated as 12-coordinated by oxygen, the volume of the (La, Nd) site can be determined from the unit-cell volume and the volume of the octahedra, as $V_{cell}/4-V_{oct}$ [42]. For all samples, as illustrated in Fig. 5 for $NdGaO_3$, the octahedra are significantly more

Table 5b
Interatomic distances, angles, and polyhedral volumes of *Pbnm* $La_{0.38}Nd_{0.62}GaO_3$ perovskite at high pressure

P (GPa)		In air	0.0001	2.007(5)	4.042(7)	5.188(8)	7.376(11)	8.462(10)	9.432(11)
Ga–O1	×2	1.9812(7)	1.9799(13)	1.9727(16)	1.9690(16)	1.9607(14)	1.9510(13)	1.9478(13)	1.9465(13)
Ga–O21	×2	1.9835(21)	1.979(4)	1.972(4)	1.964(6)	1.957(6)	1.946(7)	1.951(6)	1.946(6)
Ga–O22	×2	1.9785(19)	1.983(3)	1.966(4)	1.965(5)	1.960(5)	1.954(6)	1.949(5)	1.945(5)
$\langle GaO_6 \rangle$		1.9811(4)	1.9806(14)	1.9703(16)	1.9658(22)	1.9593(22)	1.9506(22)	1.9490(20)	1.9452(20)
V_{oct}		10.364	10.356	10.194	10.113	10.025	9.891	9.866	9.810
$V_{oct,reg}$		10.367(12)	10.359(21)	10.198(25)	10.129(34)	10.029(34)	9.895(34)	9.872(30)	9.814(30)
O1–Ga–O2	×2	90.26(10)	89.87(19)	90.56(26)	90.00(30)	90.05(28)	89.57(31)	89.47(27)	89.79(30)
O1–Ga–O2	×2	90.78(11)	90.66(19)	90.88(25)	90.68(26)	90.64(26)	90.79(26)	91.01(24)	90.53(27)
O1–Ga–O1	×2	180.00	180.00	180.00	180.00	180.00	180.00	180.00	180.00
O1–Ga–O2	×2	89.22(11)	89.34(19)	89.12(25)	89.32(26)	89.36(26)	89.21(26)	88.99(24)	89.47(27)
O1–Ga–O2	×2	89.74(10)	90.13(19)	89.44(26)	90.00(30)	89.95(28)	90.43(31)	90.53(27)	90.21(30)
O2–Ga–O2	×2	91.10(2)	91.07(4)	91.14(5)	91.30(6)	91.25(6)	91.34(6)	91.47(6)	91.43(6)
O2–Ga–O2	×2	89.74(11)	90.13(19)	89.44(27)	90.00(29)	89.95(29)	90.43(31)	90.53(28)	90.21(31)
O2–Ga–O2	×2	88.90(2)	88.93(4)	88.86(5)	88.70(6)	88.75(6)	88.6606)	88.53(6)	88.57(6)
O2–Ga–O2	×2	180.00	180.00	180.00	180.00	180.00	180.00	180.00	180.00
La(Nd)–O1 i		3.053(3)	3.038(6)	3.029(8)	2.994(10)	2.978(10)	2.946(10)	2.941(9)	2.930(10)
La(Nd)–O1 ii		2.520(3)	2.534(6)	2.514(8)	2.526(10)	2.525(9)	2.529(10)	2.524(9)	2.526(10)
La(Nd)–O1 iii		2.368(3)	2.372(6)	2.366(8)	2.350(7)	2.356(7)	2.357(7)	2.356(6)	2.344(6)
La(Nd)–O1 iv		3.120(3)	3.114(6)	3.106(8)	3.103(7)	3.088(7)	3.069(7)	3.064(6)	3.069(6)
La(Nd)–O2 v	×2	2.4044(22)	2.404(4)	2.413(5)	2.393(6)	2.392(6)	2.391(6)	2.372(6)	2.379(6)
La(Nd)–O2 vi	×2	2.6151(22)	2.615(3)	2.601(4)	2.596(5)	2.597(5)	2.583(5)	2.584(5)	2.583(5)
La(Nd)–O2 vii	×2	3.2679(23)	3.267(4)	3.225(6)	3.221(6)	3.202(6)	3.177(6)	3.183(6)	3.166(6)
La(Nd)–O2 viii	×2	2.7415(19)	2.743(3)	2.740(5)	2.740(5)	2.728(5)	2.728)5)	2.724(4)	2.717(4)
$\langle La(Nd)–O_{12} \rangle$		2.760(3)	2.760(4)	2.748(6)	2.740(7)	2.732(6)	2.721(7)	2.718(6)	2.713(6)
$\langle La(Nd)–O_8 \rangle$		2.551(3)	2.554(4)	2.549(6)	2.542(6)	2.539(6)	2.536(6)	2.530(6)	2.528(6)
$\langle La(Nd)–O_4 \rangle$		3.177(3)	3.171(5)	3.146(7)	3.135(7)	3.118(7)	3.092(7)	3.093(7)	3.083(7)
V_{dod}		47.71(3)	47.71(4)	47.24(5)	46.70(7)	46.47(7)	46.02(7)	45.78(6)	45.59(6)
Ga–O1–Ga		155.12(12)	155.48(33)	155.5(4)	155.4(4)	155.9(4)	156.8(4)	156.7(4)	156.3(4)
Ga–O2–Ga		155.82(12)	155.83(20)	157.1(3)	156.5(3)	157.0(3)	157.4(3)	156.7(3)	157.3(3)

compressible than both the unit-cell volume and the $(La, Nd)O_{12}$ site. This result is in agreement with the prediction of the bond-valence matching principle [16] which predicts that the ratio of site compressibilities $\beta_B/\beta_A = M_A/M_B$ is greater than 1 for both $LaGaO_3$ and $NdGaO_3$.

Numerical estimates of the polyhedral compressibilities or polyhedral bulk moduli of both the octahedra and the (La, Nd) sites can be obtained by fitting appropriate equations of state to the volumes of the polyhedra obtained from the structure refinements at pressure. Unfortunately, the uncertainties in the data, and the limited pressure range for some samples precludes the full refinement of all EoS parameters including K_0'. The polyhedral volume evolution with pressure was therefore fit with K_0' fixed at 4, as well as with K_0' fixed at the value obtained from fitting the EoS of the unit-cell volume. Although the exact numerical values of the polyhedral bulk moduli depend, of course, on the value chosen for K_0', all reasonable estimates and internally consistent treatments of the datasets lead to the same general conclusions. We use here the results obtained from fitting the polyhedral volumes with $K_0' = 4$ (i.e. Birch–Murnaghan second-order EoS).

The bulk moduli of the $(La, Nd)O_{12}$ site increase by less than 5% across the compositional join. This is because the four longer (La, Nd)–O bonds are stiffer while at the same time the eight shorter (La, Nd)–O bonds are softer in samples with higher Nd contents (larger x). This pattern arises from the decrease in the rate of tilting of the octahedra at larger x (Fig. 3). The most unusual result to emerge from these structure refinements is that the GaO_6 octahedra are significantly stiffer (Fig. 6) at Nd contents of $x = 0.20$ and greater, even though the room pressure volumes are larger. This is not just an artifact from angular changes within the octahedra because the maximum changes in the internal O–Ga–O angles are less than 0.5°. And the same result is seen in the Ga–O bond lengths; the Ga–O bond lengths increase with increasing x, but become stiffer (Fig. 4).

Structure refinements based upon X-ray diffraction data only provide information on the average structure, and thus structural evolution with pressure, of the octahedra. Therefore it cannot be determined whether all individual octahedra within the structure compress identically, or whether the true local structure consists of a variety of octahedral environments. Nonetheless, the plateau visible

Table 6a
Refinement information, unit cell parameters and refined positional parameters and anisotropic displacement parameters (β_{ij}) of *Pbnm* $NaGaO_3$ perovskite at high pressure

P (GPa)	0.0001	2.223(10)	3.297(10)	4.339(14)	5.314(14)	6.294(22)	7.294(10)	8.292(9)
N_{obs} ($I>2I_0/\sigma(I_0)$)	804	773	757	765	751	806	752	763
N_{ind} ($F^2>2\sigma(F^2)$)	304	288	302	296	269	271	290	285
R_{int}	0.041	0.033	0.040	0.038	0.045	0.029	0.028	0.031
G_{fit}	1.02	1.13	1.10	1.07	1.10	1.16	1.17	1.18
N_{int}	304	287	300	295	269	271	295	283
Weight, p	0.00	0.00	0.012	0.00	0.00	0.02	0.01	0.00
Extinction $\times 10^{-4}$	0.115(8)	0.098(6)	0.090(8)	0.099(8)	0.099(6)	0.151(11)	0.109(7)	0.115(7)
R_w	0.027	0.027	0.036	0.030	0.031	0.034	0.027	0.023
R_{uw}	0.024	0.025	0.030	0.027	0.027	0.028	0.021	0.022
a (Å)	5.42932(19)	5.41276(28)	5.40512(12)	5.39812(20)	5.39151(13)	5.38505(19)	5.37956(17)	5.37343(14)
b (Å)	5.49908(13)	5.47004(15)	5.45737(13)	5.44474(14)	5.43402(9)	5.42336(13)	5.41275(13)	5.40253(11)
c (Å)	7.7080(3)	7.6797(4)	7.66613(29)	7.6544(4)	7.64312(24)	7.6325(4)	7.62079(29)	7.61042(24)
V (Å^3)	230.132(13)	227.379(13)	226.134(11)	224.973(15)	223.925(9)	222.907(13)	221.904(10)	220.931(8)
La(Nd): B_{eq}	0.351(15)	0.346(17)	0.367(18)	0.371(18)	0.37(3)	0.403(10)	0.463(17)	0.434(15)
x	−0.00909(5)	−0.00863(5)	−0.00857(6)	−0.00833(6)	−0.00815(7)	−0.00799(5)	−0.00792(4)	−0.00774(4)
y	0.04134(7)	0.03991(7)	0.03929(8)	0.03851(7)	0.03803(8)	0.03738(7)	0.03681(6)	0.03628(5)
β_{11}	0.00375(12)	0.00326(12)	0.00327(18)	0.00354(14)	0.00388(16)	0.00329(14)	0.00371(12)	0.00374(11)
β_{22}	0.00388(14)	0.00410(15)	0.0041(2)	0.00417(17)	0.00448(18)	0.00394(18)	0.00442(15)	0.00421(12)
β_{33}	0.00059(17)	0.00070(18)	0.00098(19)	0.0009(3)	0.0006(3)	0.0006(3)	0.00190(19)	0.00164(16)
β_{12}	−0.00034(6)	−0.00050(7)	−0.00045(7)	−0.00052(8)	−0.00051(9)	−0.00036(5)	−0.00035(5)	−0.00041(6)
Ga: B_{eq}	0.30(3)	0.29(3)	0.24(3)	0.28(3)	0.31(3)	0.325(11)	0.347(19)	0.363(17)
β_{11}	0.0028(2)	0.0025(3)	0.0025(4)	0.0031(3)	0.0031(3)	0.0026(3)	0.0035(3)	0.00329(17)
β_{22}	0.0024(3)	0.0025(3)	0.0030(3)	0.0027(3)	0.0031(3)	0.0024(3)	0.00287(18)	0.00269(16)
β_{33}	0.0011(4)	0.0012(4)	0.0003(4)	0.0007(4)	0.0009(4)	0.0015(4)	0.0013(3)	0.0017(3)
β_{12}	−0.00001(8)	−0.00017(10)	−0.00002(11)	−0.00001(11)	0.00010(13)	−0.00003(8)	−0.00005(9)	−0.00010(8)
β_{13}	0.00004(10)	−0.00004(12)	0.00004(11)	0.00000(12)	−0.00002(15)	0.00022(11)	0.00015(8)	0.00002(8)
β_{23}	−0.00017(14)	0.00002(17)	−0.00019(19)	−0.00034(18)	−0.00009(19)	0.0002(3)	0.00009(19)	−0.00008(14)
O1: B_{eq}	0.64(6)	0.47(13)	0.42(11)	0.51(14)	0.48(17)	0.51(5)	0.68(9)	0.62(9)
x	0.0786(8)	0.0787(9)	0.0786(9)	0.0793(9)	0.0781(10)	0.0769(7)	0.0763(6)	0.0770(6)
y	0.4815(8)	0.4822(9)	0.4834(10)	0.4844(10)	0.4854(11)	0.4865(8)	0.4852(8)	0.4870(7)
β_{11}	0.0050(12)	0.0055(13)	0.0026(16)	0.0039(14)	0.0047(16)	0.0047(10)	0.0059(10)	0.0050(9)
β_{22}	0.0085(13)	0.0054(16)	0.0073(18)	0.0038(15)	0.005(3)	0.0056(11)	0.0038(12)	0.0063(11)
β_{33}	0.0013[a]	0.0006(19)	0.0003(17)	0.003(3)	0.002(3)	0.0011(17)	0.0039(15)	0.0023(13)
β_{12}	−0.0002(9)	−0.0004(10)	−0.0005(10)	−0.0007(10)	0.0011(10)	−0.0006(7)	0.0002(8)	−0.0006(7)
O2: B_{eq}	0.41(7)	0.42(9)	0.49(7)	0.47(9)	0.50(12)	0.50(4)	0.55(8)	0.45(8)
x	0.7102(5)	0.7102(5)	0.7100(6)	0.7102(6)	0.7110(7)	0.7107(5)	0.7111(4)	0.7116(4)
y	0.2894(6)	0.2902(6)	0.2902(7)	0.2895(7)	0.2888(8)	0.2892(4)	0.2892(5)	0.2888(4)
z	0.0422(6)	0.0435(6)	0.0425(6)	0.0432(7)	0.0417(8)	0.0423(6)	0.0410(6)	0.0416(6)
β_{11}	0.0052(8)	0.0037(9)	0.0037(9)	0.0047(9)	0.0048(10)	0.0048(6)	0.0040(7)	0.0038(6)
β_{22}	0.0034(9)	0.0036(10)	0.0043(10)	0.0033(9)	0.0039(11)	0.0035(8)	0.0042(7)	0.0040(6)
β_{33}	0.0009(10)	0.0016(14)	0.0022(10)	0.0019(13)	0.0020(18)	0.0020[a]	0.0030(11	0.0019(11
β_{12}	−0.0011(6)	−0.0008(7)	0.0000(8)	−0.0009(7)	−0.0017(8)	−0.0014(6)	−0.0006(6)	−0.0007(5)
β_{13}	−0.0002(5)	0.0014(6)	0.0015(7)	0.0004(6)	−0.0002(8)	0.0015(7)	0.0006(5)	0.0012(5)
β_{23}	0.0000(5)	−0.0004(7)	0.0003(7)	−0.0010(8)	0.0000(7)	−0.0005(7)	−0.0009(5)	−0.0009(5)

in the bulk moduli of the octahedra (Fig. 6) can be explained as a simple consequence of the connectivity of the perovskite structure and the difference in the compressibilities of the GaO_6 octahedra in the two end-members. Each GaO_6 octahedron has eight neighboring (La, Nd) sites. As La is initially substituted for Nd, only a small proportion of GaO_6 octahedra will therefore be softened, and the structure will continue to be supported by the stiffer GaO_6 octahedra associated with Nd neighbors. The results from the $x = 0.20$ sample show that the connectivity of the structure clearly allows the structure to remain stiff even with the octahedra "softened" by 80% La substitution. At some slightly greater La content (lower x) a percolation threshold is reached and the softer GaO_6 octahedra associated with neighboring La sites become sufficiently connected to soften the framework as a whole. Thus, for the sample with $x = 0.12$ (88% La substitution), there is an increased compressibility measurable from the average bond lengths and polyhedral volumes provided by X-ray diffraction. It is this softening of the GaO_6 octahedra, induced by La substitution for Nd, that in turn leads to the phase transition from *Pbnm* to *R-3c* symmetry in the La-rich samples [19].

Table 6b
Interatomic distances, angles, and polyhedral volumes of *Pbnm* $NdGaO_3$ perovskite at high pressure

P (GPa)		0.0001	2.223(10)	3.297(10)	4.339(14)	5.314(14)	6.294(22)	7.294(10)	8.292(9)
Ga–O1	× 2	1.9764(9)	1.9690(10)	1.9651(10)	1.9627(10)	1.9582(11)	1.9539(8)	1.9506(7)	1.9484(7)
Ga–O21	× 2	1.9808(25)	1.9720(27)	1.9681(30)	1.9673(30)	1.9613(36)	1.9593(23)	1.9534(23)	1.9502(21)
Ga–O22	× 2	1.9850(26)	1.9814(30)	1.9758(32)	1.9700(30)	1.9644(36)	1.9624(22)	1.9587(23)	1.9565(20)
$\langle GaO_6 \rangle$		1.9807(10)	1.9742(12)	1.9697(12)	1.9667(12)	1.9613(14)	1.9586(9)	1.9542(9)	1.9517(8)
V_{oct}		10.373	10.254	10.185	10.139	10.057	10.014	9.948	9.909
$V_{oct,reg}$		10.361(16)	10.259(19)	10.189(19)	10.143(19)	10.059(22)	10.017(14)	9.951(14)	9.912(12)
O1–Ga–O2	× 2	88.95(16)	88.74(17)	89.07(18)	89.10(18)	89.33(25)	89.18(15)	89.27(15)	89.39(15)
O1–Ga–O2	× 2	89.68(16)	90.03(17)	89.98(19)	90.19(19)	90.09(23)	90.48(16)	90.05(15)	90.32(15)
O1–Ga–O1	× 2	180.00	180.00	180.00	180.00	180.00	180.00	180.00	180.00
O1–Ga–O2	× 2	90.32(16)	89.97(17)	90.02(19)	89.81(19)	89.91(23)	89.52(16)	89.95(15)	89.68(15)
O1–Ga–O2	× 2	91.05(16)	91.26(17)	90.93(18)	90.90(18)	90.67(25)	90.82(15)	90.73(15)	90.61(15)
O2–Ga–O2	× 2	90.85(4)	91.09(5)	91.06(5)	91.15(5)	91.09(6)	91.18(4)	91.14(4)	91.23(4)
O2–Ga–O2	× 2	91.05(16)	91.26(18)	90.93(19)	90.90(19)	90.67(24)	90.82(16)	90.73(15)	90.61(15)
O2–Ga–O2	× 2	89.15(4)	88.91(5)	88.94(5)	88.85(5)	88.91(6)	88.82(4)	88.86(4)	88.77(4)
O2–Ga–O2	× 2	180.00	180.00	180.00	180.00	180.00	180.00	180.00	180.00
Nd–O1 i		2.360(4)	2.349(4)	2.344(5)	2.335(5)	2.336(5)	2.338(4)	2.339(3)	2.330(3)
Nd–O1 ii		2.467(4)	2.465(5)	2.469(5)	2.473(5)	2.475(6)	2.478(4)	2.469(4)	2.477(4)
Nd–O1 iii		3.110(4)	3.102(4)	3.096(5)	3.096(5)	3.086(5)	3.076(4)	3.070(3)	3.071(3)
Nd–O1 iv		3.115(4)	3.087(5)	3.070(5)	3.054(5)	3.039(6)	3.022(4)	3.020(4)	3.002(4)
Nd–O2 v	× 2	2.383(4)	2.360(4)	2.359(4)	2.352(4)	2.359(5)	2.349(3)	2.351(3)	2.346(3)
Nd–O2 vi	× 2	2.598(3)	2.590(3)	2.592(4)	2.585(4)	2.585(5)	2.583(3)	2.586(3)	2.579(3)
Nd–O2 vii	× 2	2.712(4)	2.711(4)	2.700(4)	2.703(4)	2.693(5)	2.693(3)	2.682(3)	2.684(4)
Nd–O2 viii	× 2	3.319(4)	3.309(4)	3.296(4)	3.289(4)	3.270(5)	3.268(4)	3.253(3)	3.247(3)
$\langle NdO_{12} \rangle$		2.756(3)	2.745(5)	2.739(5)	2.735(5)	2.729(5)	2.725(4)	2.720(4)	2.716(4)
$\langle NdO_8 \rangle$		2.527(3)	2.517(5)	2.514(5)	2.511(5)	2.511(5)	2.508(4)	2.506(4)	2.503(4)
$\langle NdO_4 \rangle$		3.216(3)	3.202(5)	3.189(5)	3.182(5)	3.166(5)	3.159(4)	3.149(4)	3.142(4)
V_{dod}		47.16(3)	46.59(3)	46.35(4)	46.10(4)	45.92(4)	45.70(3)	45.53(3)	45.32(2)
Ga–O1–Ga		154.34(24)	154.36(25)	154.46(27)	154.30(26)	154.73(30)	155.14(21)	155.23(18)	155.11(18)
Ga–O2–Ga		153.97(20)	153.44(22)	153.71(22)	153.63(24)	154.31(30)	154.02(21)	154.51(19)	154.44(19)

Table 7a
Refinement information, unit cell parameters and refined positional parameters and anisotropic temperature factor (β_{ij}) of $LaGaO_3$ perovskite in *R-3c* phase at high pressure

P (GPa)	2.356(7)	3.600(13)	4.749(13)	5.798(11)	7.334(14)	8.127(23)
N_{obs} ($I > 2I_0/\sigma(I_0)$)	343	325	313	319	313	308
N_{ind} ($F^2 > 2\sigma(F^2)$)	93	94	89	85	88	91
R_{int}	0.030	0.032	0.028	0.029	0.032	0.029
G_{fit}	0.72	1.14	1.16	1.13	0.95	1.03
N_{int}	92	93	89	93	88	90
Weight, p	0.0	0.0	0.0	0.0	0.0	0.0
Extinction $\times 10^{-4}$	0.051(5)	0.066(8)	0.067(8)	0.065(7)	0.067(6)	0.065(6)
R_w	0.016	0.022	0.022	0.025	0.019	0.019
R_{uw}	0.013	0.019	0.018	0.019	0.018	0.016
$a(=b)$ (Å)	5.50351(22)	5.49277(12)	5.48248(15)	5.47353(18)	5.46135(26)	5.45502(17)
c (Å)	13.2875(6)	13.2601(5)	13.2332(5)	13.2102(6)	13.1781(8)	13.1610(5)
V (Å^3)	348.54(3)	346.465(22)	344.469(23)	342.747(26)	340.39(4)	339.166(24)
La: B_{eq}	0.540(18)	0.51(3)	0.48(3)	0.50(3)	0.48(3)	0.49(3)
β_{11}	0.00494(13)	0.00504(19)	0.0049(2)	0.0048(3)	0.00470(17)	0.00459(16)
β_{33}	0.00102(8)	0.00088(11)	0.00079(10)	0.00091(12)	0.00086(10)	0.00094(9)
Ga: B_{eq}	0.34(3)	0.40(4)	0.38(5)	0.39(5)	0.39(4)	0.42(4)
β_{11}	0.00400(18)	0.0041(3)	0.0038(3)	0.0040(3)	0.0038(3)	0.0036(3)
β_{33}	0.00041(13)	0.0007(2)	0.00067(19)	0.0006(3)	0.00073(18)	0.00089(17)
O: B_{eq}	0.72(7)	0.62(9)	0.66(11)	0.79(11)	0.72(8)	0.57(8)
x	0.5575(6)	0.5579(7)	0.5561(8)	0.5562(8)	0.5567(6)	0.5565(6)
β_{11}	0.0068(6)	0.0078(9)	0.0077(10)	0.0062(9)	0.0067(8)	0.0075(9)
β_{22}	0.0055(10)	0.0060(13)	0.0072(14)	0.0048(14)	0.0066(12)	0.0072(13)
β_{33}	0.0014(4)	0.0008(5)	0.0009(5)	0.0019(6)	0.0014(4)	0.0005(5)
β_{23}	−0.0011(4)	−0.0014(5)	−0.0014(5)	−0.0011(5)	−0.0013(4)	−0.0017(4)

La: $x = 0.0$, $y = 0.0$, $z = 0.25$; $\beta_{22} = \beta_{11}$, $\beta_{12} = 0.5\beta_{11}$, $\beta_{13} = \beta_{23} = 0$.
Al: $x = 0.0$, $y = 0.0$, $z = 0.0$; $\beta_{22} = \beta_{11}$, $\beta_{12} = 0.5\beta_{11}$, $\beta_{13} = \beta_{23} = 0$.
O: $y = 0.0$, $z = 0.25$; $\beta_{12} = 0.5\beta_{22}$, $\beta_{13} = 0.5\beta_{23}$.

Table 7b
Interatomic distances, angles, and polyhedral volumes of $LaGaO_3$ perovskite in *R-3c* phase at high pressure

P (GPa)		2.356(7)	3.600(13)	4.749(13)	5.798(11)	7.334(14)	8.127(23)
Ga–O	× 6	1.9622(5)	1.9586(6)	1.9534(6)	1.9501(7)	1.9462(5)	1.9436(5)
V_{oct}		10.065	10.011	9.930	9.881	9.821	9.783
$V_{oct,reg}$		10.073(8)	10.018(9)	9.938(9)	9.888(11)	9.828(8)	9.789(8)
O–Ga–O		91.28(1)	91.29(2)	91.26(2)	91.26(2)	91.28(1)	91.28(1)
Nd–O1 i	× 3	2.436(3)	2.429(4)	2.434(4)	2.429(4)	2.421(3)	2.419(3)
Nd–O2 ii	× 6	2.7438(3)	2.7385(4)	2.7320(4)	2.7274(5)	2.7213(4)	2.7178(4)
Nd–O2 iii	× 3	3.0679(28)	3.064(4)	3.049(4)	3.044(4)	3.040(4)	3.036(3)
ω		11.27(5)	11.34(6)	11.00(7)	11.02(7)	11.11(5)	11.07(5)
η		0.9667	0.9663	0.9673	0.9671	0.9666	0.9666
V_{dod}		48.02(4)	47.73(4)	47.48(4)	47.24(4)	46.91(4)	46.75(4)

Table 8a
Refinement information, unit cell parameters and refined positional parameters and anisotropic displacement parameters (β_{ij}) of $La_{0.88}Nd_{0.12}GaO_3$ perovskite in *R-3c* phase at high pressure

P (GPa)	8.020(2)	9.496(13)
N_{obs} ($I > 2I_0/\sigma(I_0)$)	309	331
N_{ind} ($F^2 > 2\sigma(F^2)$)	78	86
R_{int}	0.045	0.034
G_{fit}	0.89	0.98
N_{int}	78	86
Weight, p	0.0	0.0
Extinction $\times 10^{-4}$	0.052(7)	0.051(5)
R_w	0.023	0.021
R_{uw}	0.020	0.017
$a(=b)$ (Å)	5.4524(3)	5.4414(5)
c (Å)	13.1452(9)	13.1211(17)
V (Å^3)	338.44(4)	336.45(7)
La: B_{eq}	0.56(3)	0.470(17)
β_{11}	0.0065(3)	0.00496(19)
β_{33}	0.00077(10)	0.00077(7)
Ga: B_{eq}	0.43(4)	0.35(3)
β_{11}	0.0051(5)	0.0038(3)
β_{33}	0.00057(17)	0.00055(12)
O: B_{eq}	0.78(12)	0.70(10)
x	0.5559(11)	0.5566(8)
β_{11}	0.0098(13)	0.0074(10)
β_{22}	0.0075(19)	0.0051(15)
β_{33}	0.0011(6)	0.0013(5)
β_{23}	−0.0012(6)	−0.0011(5)

Table 8b
Interatomic distances, angles, and polyhedral of $La_{0.88}Nd_{0.12}GaO_3$ perovskite in *R-3c* phase at high pressure

P (GPa)		8.020(2)	9.496(13)
Ga–O	× 6	1.9417(9)	1.9385(7)
V_{oct}		9.754	9.705
$V_{oct,reg}$		9.761(14)	9.712(11)
O–Ga–O		91.30(2)	91.30(2)
Nd–O1 i	× 3	2.421(5)	2.413(4)
Nd–O2 ii	× 6	2.7148(6)	2.7101(5)
Nd–O2 iii	× 3	3.031(5)	3.029(4)
ω		11.09(8)	11.09(16)
η		0.9659	0.9661
V_{dod}		46.605	46.371

3.3. Phase transition

A previous single-crystal X-ray diffraction study [19] confirmed that $LaGaO_3$ undergoes a first-order phase transition from *Pbnm* to *R-3c* symmetry at 2.3 GPa, as first observed in a powder diffraction experiment [23]. The same transition was found in the sample with $x = 0.06$ and 0.12 by single-crystal diffraction. It is clearly marked by a discontinuity in the unit-cell volume (Fig. 1). The transition at ~5.8 GPa in the $x = 0.06$ sample resulted in broadening of the X-ray diffraction peaks that precluded a full data collection and refinement. Nonetheless, the measured cell parameters, peak intensities and systematic absences are consistent with it having *R-3c* symmetry. Careful reversals of the transition in the $x = 0.12$ sample show that the transition pressure lies between 7.712(5) and 7.91(2) GPa, and structure refinement (Table 8) has confirmed that the high-pressure phase has *R-3c* symmetry.

The transition is also apparent in the Raman spectra of these three samples. As for the transition at high temperatures [26,35] it is accompanied by a decrease in the number of vibration bands, as expected for this symmetry change. The transition pressure for the $x = 0.20$ sample exceeded the maximum pressure attainable in our diamond-anvil cells used for single-crystal diffraction experiments, but the transition was found by Raman spectroscopy alone at ~12 GPa. No evidence of the transition in $NdGaO_3$ was detected in Raman measurements up to 16 GPa. These data show that the transition pressure increases with increasing Nd content (increasing x) at approximately 0.45 GPa per 0.01 increment in x, at least up to $x = 0.20$, but there is no information on the further evolution of the transition pressure for $x > 0.20$. Linear extrapolation would suggest a transition pressure of about 50 GPa for $NdGaO_3$, but in view of the plateau effect in the octahedral compressibilities noted above, this must represent a maximum estimate and the transition may well be expected to occur at much lower pressures.

Table 9
Unit cell parameters of $La_{1-x}Nd_xGaO_3$ perovskite at different pressures

$x = 0.00$ *Pbnm*	P (GPa)	0.0001	0.117(4)	0.254(5)	0.566(5)	0.897(5)	1.287(5)	2.151(6)			
	a (Å)	5.52323(9)	5.52245(11)	5.52125(10)	5.51894(12)	5.51647(12)	5.51353(12)	5.50734(22)			
	b (Å)	5.49032(22)	5.48905(27)	5.48772(23)	5.48425(28)	5.48034(29)	5.47561(28)	5.4651(6)			
	C (Å)	7.77542(7)	7.77364(16)	7.77101(14)	7.76569(17)	7.75986(17)	7.75320(17)	7.73997(42)			
	V (Å^3)	235.784(07)	235.642(16)	235.454(14)	235.046(17)	234.597(13)	234.069(13)	232.958(29)			
$x = 0.00$ *R-3c*	P (GPa)	2.356(7)	2.711(9)	3.600(11)	4.058(11)	4.749(13)	5.798(11)	6.679(19)	7.334(14)	8.127(23)	
	a (Å)	5.50351(22)	5.5005(3)	5.49277(16)	5.48828(21)	5.48248(15)	5.47353(18)	5.46637(20)	5.46135(26	5.45502(17)	
	c (Å)	13.2875(6)	13.2794(9)	13.2601(5)	13.2483(6)	13.2332(5)	13.2102(6)	13.1928(6)	13.1781(8)	13.1610(5)	
	V (Å^3)	348.54(3)	348.02(4)	346.465(22)	345.588(29)	344.469(23)	342.747(26)	341.403(27)	340.39(4)	339.166(24)	
$x = 0.06$ *Pbnm*	P (GPa)	0.0001	0.967(2)	2.56(5)*	3.98(5)*	5.30(5)*		0.001$^+$	0.545(2)$^+$	1.065(3)$^+$	1.859(3)$^+$
	a (Å)	5.5124(5)	5.5054(4)	5.4980(5)	5.4870(4)	5.47895(27)		5.5143(5)	5.5104(5)	5.5065(5)	5.5009(6)
	b (Å)	5.49360(20)	5.48190(20)	5.4625(9)	5.4445(6)	5.43108(24)		5.49220(21)	5.48558(20)	5.47938(20)	5.47059(27)
	c (Å)	7.7706(8)	7.7547(9)	7.7327(17)	7.7067(15)	7.6837(8)		7.7709(8)	7.7618(8)	7.7535(8)	7.7397(8)
	V (Å^3)	235.32(4)	234.04(3)	232.23(6)	230.23(5)	228.640(26)		235.35(3)	234.62(3)	233.94(3)	232.913(4)
$x = 0.12$ *Pbnm*	P (GPa)	0.0001	0.661(1)	0.885(2)	1.346(1)	1.971(3)	2.593(4)	3.549(3)	4.497(6)	5.213(8)	6.437(7)
	a (Å)	5.51278(36)	5.50750(32)	5.50569(33)	5.50235(28)	5.49867(26)	5.49367(31)	5.48769(25)	5.48116(29)	5.47626(21)	5.46878(23)
	b (Å)	5.4928(4)	5.4845(5)	5.4817(4)	5.4761(4)	5.4693(4)	5.4627 (4)	5.4519(4)	5.4425(4)	5.43536(2.9)	5.42351(31)
	c (Å)	7.7732(7)	7.7618(7)	7.7578(6)	7.7498(6)	7.73915(5)	7.7284(6)	7.7141(5)	7.6997(5)	7.6886(4)	7.6695 (4)
	V (Å^3)	235.375(29)	234.449(27)	234.133(25)	233.513(23)	232.747(21)	231.932(24)	230.793(20)	229.691(23)	228.855(17)	227.477(18)
	P (GPa)	7.216(6)	7.250(5)	7.354(4)	7.574(4)	7.712(5)					
	a (Å)	5.46497(38)	5.46396(38)	5.46358(37)	5.4621(5)	5.4610(5)					
	b (Å)	5.4160(4)	5.4160(7)	5.41464(38)	5.4126(4)	5.4114(5)					
	c (Å)	7.6599(6)	7.6590(10)	7.6573(5)	7.6543(5)	7.6524(7)					
	V (Å^3)	226.722(23)	226.65(4)	226.525(22)	226.293(27)	226.141(29)					
$x = 0.20$ *Pbnm*	P (GPa)	0.0001	0.398(4)	1.217(4)	2.187(3)	3.228(5)	5.192(4)	6.650(3)	7.737(18)	8.166(8)	
	a (Å)	5.50601(20)	5.50282(19)	5.49676(22)	5.48952(17)	5.48238(21)	5.46909(22)	5.45984(21)	5.4537(9)	5.45111(27)	
	b (Å)	5.49275(23)	5.48790(22)	5.47778(26)	5.46713(19)	5.45517(23)	5.43496(25)	5.42043(25)	5.4101(13)	5.4066(3)	
	c (Å)	7.7673(4)	7.7608(4)	7.7490(4)	7.7329(3)	7.7164(4)	7.6878(4)	7.6669(4)	7.6462(5)	7.6463(5)	
	V (Å^3)	234.906(14)	234.368(13)	233.317(15)	232.079(11)	230.774(14)	228.512(15)	226.898(14)	225.75(7)	225.349(19)	
$x = 0.62$ *Pbnm*	P (GPa)	0.0001	0.598(5)	1.162(5)	2.007(5)	2.628(7)	4.042(7)	5.188(8)	6.322(8)	7.376(11)	8.462(10)
	a (Å)	5.4614(6)	5.4574(6)	5.4528(6)	5.4466(6)	5.4417(6)	5.4322(5)	5.4238(6)	5.4160(4)	5.4094(5)	5.4029(5)
	b (Å)	5.4961(6)	5.4887(6)	5.4806(5)	5.4697(5)	5.4626(6)	5.4457(6)	5.4325(6)	5.4201(4)	5.4092(5)	5.3989(5)
	c (Å)	7.73893(28)	7.73118(28)	7.72313(28)	7.71152(25)	7.70328(28)	7.68457(24)	7.67049(28)	7.65657(22)	7.64420(28)	7.63119(27)
	V (Å^3)	232.295(20)	231.577(20)	230.802(20)	229.733(19)	228.988(20)	227.327(18)	226.008(18)	224.763(16)	223.677(19)	222.601(19)
9.432(11)	$x = 1.00$ *Pbnm*	P (GPa)	0.0001	0.710(6)	1.486(7)	2.244(7)	3.736(10)	5.173(10)	7.401(11)	8.056(9)	
5.3968(4)		a (Å)	5.42709(24)	5.42175(34)	5.41791(34)	5.41088(41)	5.40026(32)	5.39021(20)	5.3761(4)	5.3728 (3)	
5.3890(5)		b (Å)	5.49871(10)	5.48939(14)	5.47837(21)	5.46921(23)	5.45184(13)	5.4352 (25)	5.41142(18)	5.40457(14)	
7.62046(25)		c (Å)	7.70865(13)	7.69918(19)	7.68923(19)	7.67884(23)	7.66162(17)	7.64487(14)	7.62084(22)	7.61377(17)	
221.630(17)		V (Å^3)	230.042(10)	229.144(14)	228.226(16)	227.242(17)	225.569(13)	223.971(11)	221.706(07)	221.086(12)	

Pressure data marked with (*) were determined by using ruby R1 line shift and pressures for other data were determined by internal quartz calibrant. The data marked with ($^+$) were determined for the second crystal with $x = 0.06$.

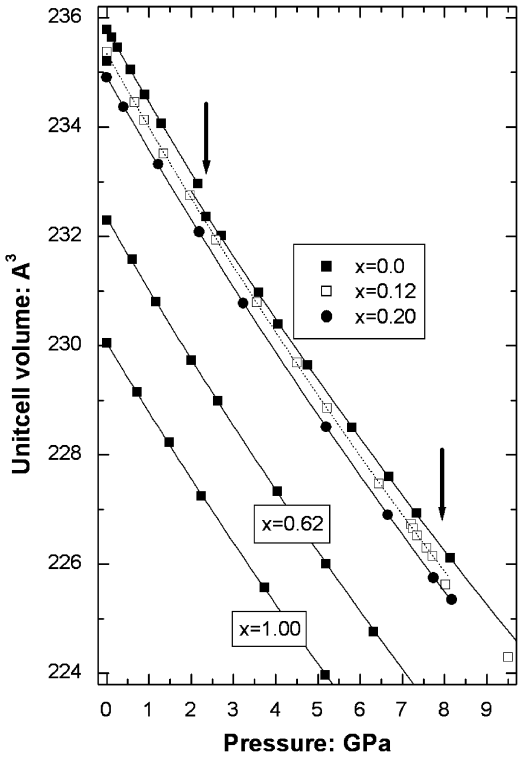

Fig. 1. The variation of the unit-cell volumes of (La, Nd)GaO_3 perovskites with pressure. The volumes of the *R-3c* phases have been multiplied by $\frac{2}{3}$ to put them on the same scale. The data for the $x = 0.06$ sample are omitted for clarity. Symbol sizes exceed the estimated uncertainties in measurements. The lines are the equations of state fit to the data. The phase transition pressures of the $x = 0.00$ and 0.12 compositions are indicated by the vertical arrows.

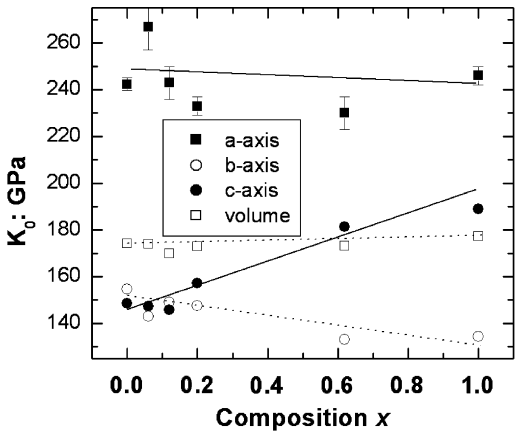

Fig. 2. The variation of bulk and linear moduli with composition in the system $La_{(1-x)}Nd_xGaO_3$ as determined from the fit of third-order Birch–Murnaghan EoS to the unit-cell parameter and volume variation with pressure. The constraints used in some fits, and the EoS parameters, are listed in Table 10. The lines are drawn as guides to the eye. Symbol sizes exceed esd's for all moduli except those for the *a*-axis.

The transition is accompanied by a 0.23% decrease in unit-cell volume in $LaGaO_3$ [19] and is decreased to ~0.1% for the $x = 0.12$ sample. The volume change arises from

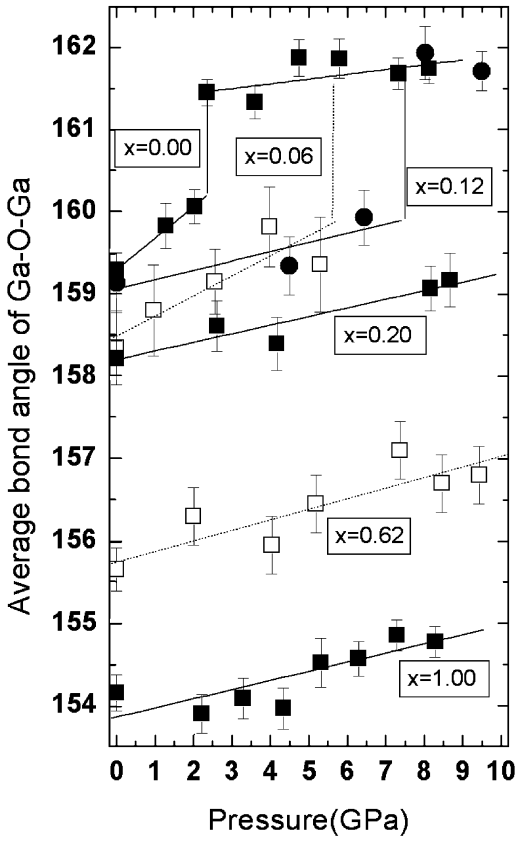

Fig. 3. Variation of the average Ga–O–Ga angle with pressure for all six samples (La, Nd)GaO_3. For the *Pbnm* structures the value plotted is $[(Ga–O_1–Ga)+2(Ga–O_2–Ga)]/3$ to account for the multiplicities of the bond angles. For the *R-3c* structures there is only one symmetrically distinct Ga–O–Ga angle. Note that the rate of increase of the average angle within the *Pbnm* phase decreases with increasing Nd content (increasing *x*). Lines are linear fits to the data.

two competing structural contributions. At the phase transition the average tilt angles of the octahedra decrease, as evidenced by the increase in average Ga–O–Ga angles (Fig. 3). Were the octahedra to be rigid through the phase transition this "un-tilting" would contribute an increase in the unit-cell volume [19]. Instead, the unit-cell volume is decreased by a 0.8% compression of the octahedra in $LaGaO_3$. The decrease in the step size of the transition at $x = 0.12$ comes from changes in both contributions. The slower rate of increase in the average $\langle$Ga–O–Ga$\rangle$ angles within the *Pbnm* structure (Fig. 3) leads to a larger jump in $\langle$Ga–O–Ga$\rangle$ angles and hence octahedral tilts, at the transition. This contributes a larger positive volume change. At the same time the octahedral volume change at the phase transition is reduced to 0.6%. This trend suggests that the transition character may change from first order to continuous at higher Nd contents (higher *x*). This weakening of the transition with increasing Nd content is also found at high temperatures, where the transition loses its first-order character at $x > 0.05$ and becomes smeared-out over a temperature interval of 20–30 K for $0.05 < x < 0.20$ [26].

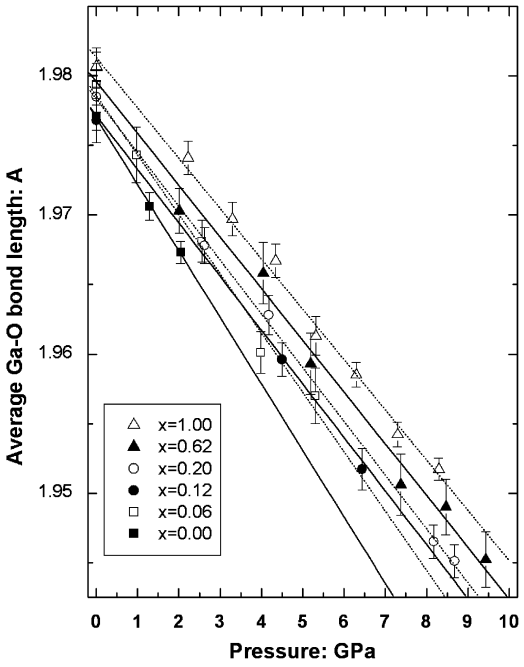

Fig. 4. Variation of average ⟨Ga–O⟩ bond lengths with pressure. Note that the shorter bond lengths in the La-rich samples (lower x) are more compressible than the longer ⟨Ga–O⟩ bond lengths in the Nd-rich samples. Lines are linear fits to the data.

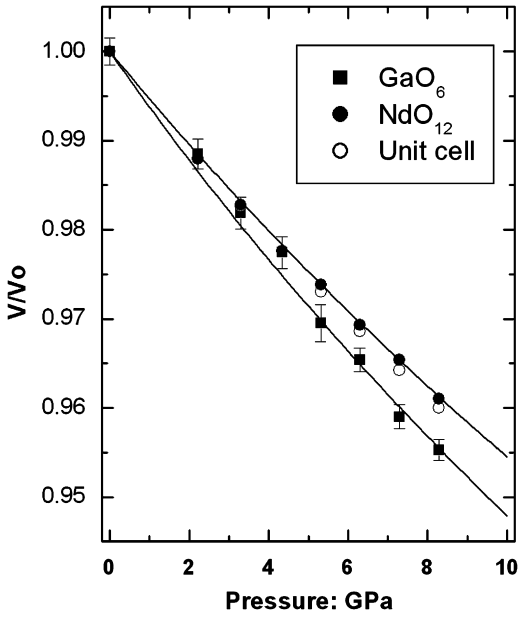

Fig. 5. The evolution of the normalized polyhedral volumes and unit-cell volume with pressure for $NdGaO_3$, showing that the octahedron is more compressible than both the structure as a whole and the NdO_{12} site. Lines are the fits to the data of Birch–Murnaghan third-order equations of state.

3.4. *R-3c* structures

Because of the rapid increase in transition pressure with compositional parameter x, we only have extensive data for $LaGaO_3$ from which to determine the high-pressure

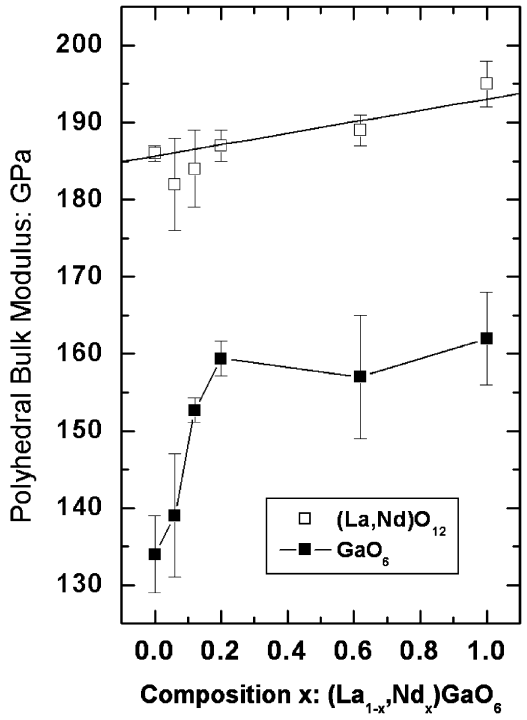

Fig. 6. Polyhedral bulk moduli for the $(La, Nd)O_{12}$ and the GaO_6 sites calculated by fitting the pressure-induced variation of the individual polyhedral volumes with a Birch–Murnaghan second-order EoS (i.e. with $K' = 4$). The line for the $(La, Nd)O_{12}$ site is a linear fit to the data.

behavior of the *R-3c* phase. The refined structures indicate that there is very little significant evolution of the structure of $LaGaO_3$ from the phase transition at ~2.2 GPa up to the maximum pressure that we achieved of 8.127(23) GPa. Unlike the high-pressure evolution of the *R-3c* phase of $LaAlO_3$ [15] there is only a small change in the ratio of the cell parameters $c/a\sqrt{3}$ that is a measure of the distortion of the structure from cubic symmetry [43]. Also in contrast to $LaAlO_3$, which shows a steady increase in Al–O–Al angles corresponding to a clear decrease of the tilts of the octahedra, there is no significant change in the tilts of the GaO_6 octahedra in $LaGaO_3$ (Table 7b). The reason for this difference in behavior between $LaGaO_3$ and $LaAlO_3$ arises from differences in the compressibilities of the corresponding octahedra. In *R-3c* perovskites there is a direct relationship between the ratio of the polyhedral volumes and the tilt angle [44] from which can be derived the result that the rate of tilting with pressure increases with an increase in the difference between the compressibilities of the AO_{12} and BO_6 polyhedra [15]. The experimental data show that whereas the AlO_6 octahedra are significantly softer than the LaO_{12} sites in $LaAlO_3$, and this drives the *R-3c* structure towards the phase transition to cubic at pressures in excess of 14 GPa [18], the GaO_6 and LaO_{12} sites in the *R-3c* phase of $LaGaO_3$ have almost identical compressibilities within our experimental uncertainties. Thus the polyhedral tilts in $LaGaO_3$ do not change significantly over our experimental pressure range. The

Table 10
Bulk and linear moduli of $La_{1-x}Nd_xGaO_3$ perovskites

Composition: x	0.00	0.06	0.12	0.20	0.62	1.00
N data[a]	7	5	15	9	11	8
P_{max} (GPa)	2.151	5.30	7.712	8.166	9.432	8.056
Volume						
V_o	235.790(6)	235.319(22)	235.350(19)	234.912(11)	232.328(17)	230.048(15)
K_o	172.4(1.2)	169(4)	169.8(1.7)	173.0(1.2)	173.1(1.4)	177.3(1.8)
K_p	6.4(fixed)	6.4(fixed)	6.6(5)	6.0(4)	6.2(4)	6.7(6)
a-axis						
a_o	5.52326(6)	5.5126(9)	5.51257(26)	5.50600(15)	5.4618(4)	5.42748(54)
K_{ao}	238(3)	267(10)	243(7)	233(4)	230(7)	234(18)
K_p	9 (fixed)	9.0 (fixed)	9.0(1.7)	10.2(1.2)	7.5(1.8)	7.7(3.9)
b-axis						
b_o	5.49060(17)	5.49378	5.49246(30)	5.49276(17)	5.4964(4)	5.49870(17)
K_{bo}	153(3)	137.7(1.9)	149(3)	147.5(1.8)	133(3)	134.3(1.7)
K_p	6.3 (fixed)	6.3 (fixed)	6.8(8)	6.5(5)	6.3(7)	5.7(6)
c-axis						
c_o	7.77547(9)	7.7713(9)	7.7731(5)	7.76751(32)	7.73927(20)	7.70865(16)
K_{co}	147.5(1.3)	143.8(2.7)	145.9(2.6)	159.1(2.5)	181.3(1.6)	189.0(2.0)
K_p	5.4 (fixed)	5.4 (fixed)	5.0(7)	3.4(7)	4.9(4)	7.5(7)

[a] N: the number of data.

same behavior is found for the $x = 0.12$ sample from 8.0 to 9.4 GPa (Table 8b).

4. Conclusions

These overall patterns of compression of the structures of (La, Nd)GaO_3 *Pbnm* perovskites and the phase transitions to the *R-3c* structure cannot be explained in terms of the more simple models of the perovskite structure based upon the treatment of the octahedra as rigid bodies. Were the octahedra to be rigid, then the tilts would increase with increasing pressure (the Ga–O–Ga bond angles would decrease), the structures would become more distorted with pressure and no phase transitions to the *R-3c* structure would take place. What we have demonstrated in this study is that, as in pure end members, the relative compressibilities of the octahedra and the extra-framework cation site of perovskites determines both their structural evolution with pressure and their possible phase transitions at high pressures, in agreement with the principle of bond-valence matching [16]. Further, we have shown that a given polyhedron such as GaO_6 does not have physical properties independent of the structure, even within a solid solution with a single structure type. Instead the compressibility of a given octahedral type, in this case GaO_6, varies with composition in perovskites as a consequence of the bond-valence matching principle. Thus, in the series $(La_{1-x}Nd_x)GaO_6$ the site parameter ratio $\beta_B/\beta_A = M_A/M_B$ decreases from 1.22 in $NdGaO_3$ to 1.18 in $LaGaO_3$. The substitution of La for Nd in the series $(La_{1-x}Nd_x)GaO_6$ thus leads to both a softening of the GaO_6 octahedra as a consequence of having to match the bond valence of the (La, Nd) site, as well as an increase in tilt rate of the octahedra when pressure is applied (see Fig. 5 in [16]). These changes in the rates of compression of the structure, in particular the octahedral softening, in turn lead directly to the reduction of the pressure of the *Pbnm* to *R-3c* phase transition because the mechanism of the transition itself requires the compression of the octahedra [19].

Acknowledgments

The authors acknowledge with gratitude the financial support for this work derived from NSF Grant EAR-0408460 to N.L. Ross and R.J. Angel. Ruby pressure determinations and Raman measurements were conducted with the Raman system in the Vibrational Spectroscopy Laboratory in the Department of Geosciences at Virginia Tech. C. Jakeways was supported by the EPSRC in the UK.

References

[1] D.W. Cooke, E.R. Gray, R.J. Houlton, B. Rusnak, E.A. Meyer, J.G. Beery, D.R. Brown, F.H. Garzon, I.D. Raistrick, A.D. Rollet, R. Bolmaro, Appl. Phys. Lett. 55 (1989) 914.
[2] G. Koren, A. Gupta, E.A. Giess, A. Segmüller, R.B. Laibowitz, Appl. Phys. Lett. 54 (1989) 1054.
[3] N. Takahashi, A. Koukitu, H. Seki, J. Mater. Sci. Lett. 17 (1998) 877.
[4] E.V. Tsipis, V.V. Kharton, J.R. Frade, P. Nùñnez, J. Solid State Electrochem. 9 (2005) 547.
[5] P.B. Mozhaev, J.E. Mozhaeva, I.K. Bdikin, I.M. Kotelyanskii, V.A. Luzanov, S.G. Zybtsev, J.B. Hansen, C.S. Jacobsen, Physics C 435 (2006) 23.
[6] D. Andrault, J.P. Poirier, Phys. Chem. Miner. 18 (1991) 91.
[7] M. O'Keeffe, B. Hyde, J.O. Bovin, Phys. Chem. Miner. 4 (1979) 299.
[8] N.L. Ross, Phys. Chem. Miner. 25 (1998) 597.
[9] N.L. Ross, R.M. Hazen, Phys Chem. Miner 17 (1990) 228.

[10] N.L. Ross, High-pressure, high temperature crystal chemistry, in: R.M. Hazen, R.T. Downs (Eds.), Reviews in Mineralogy and Geochemistry, vol. 41, Mineralogical of Society America, Washington, DC, 2000, pp. 257–287.
[11] N.L. Ross, J. Zhao, R.J. Angel, J. Solid State Chem. 177 (2004) 3768.
[12] N.L. Ross, J. Zhao, R.J. Angel, J. Solid State Chem. 177 (2004) 1276.
[13] N.L. Ross, J. Zhao, J.B. Burt, T.D. Chaplin, J. Phys.: Condens. Matter 16 (2004) 5721.
[14] J. Zhao, N.L. Ross, R.J. Angel, Phys. Chem. Miner. 31 (2004) 299.
[15] J. Zhao, N.L. Ross, R.J. Angel, J. Phys.: Condens. Matter 16 (2004) 8763.
[16] J. Zhao, N.L. Ross, R.J. Angel, Acta Crystallogr. B 60 (2004) 263.
[17] J. Zhao, N.L. Ross, R.J. Angel, Acta Crystallogr. B 62 (2006) 431.
[18] P. Bouvier, J. Kreisel, J. Phys.: Condens. Matter 14 (2002) 3981.
[19] R.J. Angel, J. Zhao, N.L. Ross, Phys. Rev. Lett. 95 (2005) 025501–025503.
[20] I.D. Brown, D. Altermatt, Acta Crystallogr. B 41 (1985) 244.
[21] I.D. Brown, Acta Crystallogr. B 48 (1992) 553.
[22] I.D. Brown, The Chemical Bond in Inorganic Chemistry. The Bond Valence Model, Oxford University Press, Oxford, 2002.
[23] B.J. Kennedy, T. Vogt, C.D. Martin, J.B. Parise, J.A. Hriljac, J. Phys.: Condens. Matter 13 (2001) L925.
[24] M. Berkowski, J. Fink-Finowicki, W. Piekarczyk, L. Perchuć, P. Byszewski, L.O. Vasylechko, D.I. Savytskij, K. Mazur, J. Sass, E. Kowalska, J. Kapuśniak, J. Cryst. Growth 209 (2000) 75.
[25] P. Byszewski, E. Kowalska, R. Diduszko, R. Aleksiyko, M. Berkowski, J. Fink-Finowicki, J. Kapuśniak, J. Thermal Anal. Calorimetry 65 (2001) 545.
[26] M.L. Sanjuán, V.M. Orera, R.I. Merino, J. Blasco, J. Phys.: Condens. Matter 10 (1998) 11687.
[27] A. Senyshyn, L. Vasylechko, M. Knapp, U. Bismayer, M. Berkowski, A. Matkovskii, J. Alloy Compd. 382 (2004) 84–91.
[28] R. Miletich, D.R. Allan, W. Kuhs, Rev. Mineral. Geochem. 41 (2000) 445.
[29] H.K. Mao, J. Xu, P.M. Bell, J. Geophys. Res. 91 (1986) 4673.
[30] R.J. Angel, D.R. Allan, R. Miletich, L.W. Finger, J. Appl. Crystallogr. 30 (1997) 461.
[31] R.J. Angel, J Appl. Crystallogr. 36 (2003) 295.
[32] L.W. Finger, H.E. King, Am. Mineral. 63 (1978) 337.
[33] R.J. Angel, J Appl. Crystallogr. 37 (2004) 486.
[34] L.W. Finger, E. Prince, A system of Fortran IV computer program for crystal structure computations. United State National Bureau of Standards, NBS Technical note, 854, Washington, DC, 1975.
[35] G.A. Tompsett, N.M. Sammes, R.J. Phillips, A.M. Cartner, J. Raman Spectroscopy 30 (1999) 497.
[36] T. Tohei, A. Kuwabara, T. Yamamoto, F. Oba, I. Tanaka, Phys. Rev. Lett. 94 (2005) 035502.
[37] J.D.C. McConnell, C.A. McCammon, R.J. Angel, F. Seifert, Zeit. Kristallogr. 215 (2000) 669.
[38] R.J. Angel, Some practical aspects of studying equations of state and structural phase transitions at high pressure, in: A. Katrusiak, P.F. McMillan (Eds.), High-Pressure Crystallography, Kluwer Academic, Dordrecht, 2004, pp. 21–36.
[39] F. Birch, Phys. Rev. 71 (1947) 809.
[40] A.I. Krivchikov, B.Ya. Gorodilov, I.G. Kolobov, A.I. Érenburg, D.I. Savitskiĭ, S.B. Ubizskiĭ, I.M. Syvorotka, L.O. Vasilechko, Low Temp. Phys. 26 (2000) 370.
[41] R.J. Angel, High-pressure, high temperature crystal chemistry, in: R.M. Hazen, R.T. Downs (Eds.), Reviews in Mineralogy and Geochemistry, vol. 41, Mineralogical of Society America, Washington, DC, 2000, pp. 35–59.
[42] N.W. Thomas, Acta Crystallogr. B 45 (1989) 337.
[43] H.D. Megaw, C.N.W. Darlington, Acta Crystallogr. A 31 (1975) 161.
[44] N.W. Thomas, A. Beitollahi, Acta Crystallogr. B 50 (1994) 549.